AIAA JOURNAL
Vol. 43, No. 9, September 2005

Consistent Third-Order Shell Theory with Application to Composite Circular Cylinders

R. A. Arciniega* and J. N. Reddy†
Texas A&M University, College Station, Texas 77843-3123

A consistent third-order shell theory with applications to composite circular cylinders is presented and its finite element formulation is developed. The formulation has seven displacement functions and requires C^0 continuity in the displacement field. The exact computation of stress resultants is carried out through numerical integration of material stiffness coefficients of the laminate. A displacement finite element model is developed using Lagrange elements with higher-order interpolation polynomials. These elements preclude any effect of shear and membranes locking. Comparisons of the present results with those found in the literature for typical benchmark problems involving isotropic and composite cylindrical shells are found to be excellent and show the validity of the developed shell theory and its implementation into a finite element code.

Introduction

SHELL structures have always been a fascinating area of research. Their unpredictable behavior and difficulties in their mathematical as well as numerical modeling make these structures a challenge for researchers and engineers. Because shells abound in nature, it is not surprising that they have been widely used as efficient load-carrying members in many engineering structures. Examples of shell applications include storage tanks, roofs, lenses, and helmets, and they are also found in automobile, aircraft, and off-shore structures.

Most significant advances in shell analyses have been made using the finite element method. Finite elements used for shells can be grouped into four kinds: flat facet element, solid three-dimensional element, degenerate element, and two-dimensional element based on a shell theory. Among these, the last two elements are the most common ones. The degenerate shell element approach was first developed by Ahmad et al.[1] from a three-dimensional solid element by a process which directly discretizes the three-dimensional elasticity equations in terms of midsurface nodal variables. On the other hand, elements based on shell theories began to appear in the late 1960s. These elements are based on convected curvilinear coordinates and are capable of capturing the membrane-bending coupling correctly. Even though degenerated approaches have dominated shell analysis during the 1970s and 1980s, beginning with the work of Simo and Fox,[2] shell elements have been increasingly used in the last decade. Examples of these formulations can be found by Chinosi et al.,[3] Cho and Roh,[4] and Chapelle et al.[5] A comparison between both methodologies was presented by Büchter and Ramm.[6]

Shell theories are developed using mainly two approaches: first, the direct approach in which the shell is considered as a two-dimensional manifold, called the Cosserat continuum (see Refs. 2 and 7–9). Interestingly, the kinematic assumptions associated with this description of the shell are equivalent to the usual first-order approximation hypothesis. The second approach is the derivation from the three-dimensional continuum theory, so-called single-layer theories.[10] In this case, the three-dimensional continuum is reduced to a two-dimensional one through a Taylor expansion of the displacement field. Of course, this idea is by far not unique. The theory chosen depends on the respective mechanical assumptions. The classical Kirchhoff–Love theory, the first-order shell theory, and the refined third-order shell theory of Reddy[11] and Reddy and Liu[12] provide fine examples of this approach.

Single-layer third or higher-order shear deformation theories are capable of predicting accurately the global behavior of plates and shells. To evaluate detailed local stress analysis, two refined theories are available: the layerwise theory and the zigzag theory. In the layerwise plate theory proposed by Reddy,[13] the three-dimensional displacement field is expanded as a linear combination of the thickness coordinate and undetermined functions of position of each layer. The continuity of the transverse normal and shear stresses is not enforced. On the other hand, in the zigzag theory[14,15] the displacement field fulfills a priori the static and geometric continuity conditions between contiguous layers.

A significant number of analytical studies for composite shells have been carried out in the last few years. Among them, we can refer to Varadan and Bhaskar[16] and Ren[17] for exact solutions of laminated cylindrical shells, Xavier et al.[18] and Cheng et al.[19] for analytical solutions of composite shells using the zigzag model, and recently, under similar kinematic assumptions, Kim and Cho[20] for linear buckling problems with multiple delaminations of composite shells.

An important question arises regarding the adoption of a kinematical model to analyze composite shells: Which model can better describe the shell behavior? It has been demonstrated that the classical shell theory is not able to predict the deformation behavior with sufficient accuracy in composite shells.[10] However, the benefits in using high-order theories instead of the first-order theory are not clearly established. One disadvantage attributed to the refined third-order theory is the presence of the first partial derivatives of the transverse displacement in the displacement field, which requires Hermite interpolation of the transverse deflection in finite element implementations. C^1-continuity elements are numerically inconvenient because they involve second partial derivatives of the interpolation functions and cannot account for all rigid-body modes of a curved element.[21,22] One way to deal with this problem was proposed by Başar et al.[23] They used a third-order theory with seven independent parameters in which no vanishing shear strain on laminate faces is required. (Also see Balah and Al-Ghamedy.[24]) Consequently, the C^0-continuity finite element was employed in their formulation. Another approach is to reduce the C^1-continuity displacement field by means of two additional functions, called warping functions.[25] The relaxation of the continuity in the displacement field leads to a third-order theory with seven parameters.

Finite elements based on shell theories are known to have locking problems due to inconsistencies in the modeling of transverse shear energy and membrane energy. The locking is avoided in many cases

Received 20 November 2003; revision received 2 March 2005; accepted for publication 28 March 2005.

*Graduate Research Assistant, Department of Mechanical Engineering; rarciniega@tamu.edu.

†Distinguished Professor, Department of Mechanical Engineering; jnreddy@shakti.tamu.edu. Associate Fellow AIAA.

by using uniformly reduced integration in the numerical evaluation of the stiffness coefficients.[26,27] Alternatively, mixed formulations with lower-order elements have been proposed to mitigate the effects of shear and membrane locking. Among them, we can cite the assumed strain elements[28,29] and the enhanced strain elements.[30] Recently, Pontaza and Reddy[31] have shown that higher-order elements using spectral interpolation are free of shear locking, insensitive to geometric distortions, and can accurately predict displacements as well as stress resultants in the entire domain of the plate. A similar idea was already applied for cylindrical shells by Chinosi et al.[3]

The purpose of this paper is to propose a consistent third-order shear deformation theory for the analysis of multilayered composite shells. The formulation, based on the ideas of Reddy and Liu,[12] has seven parameters with C^0 continuity in the displacement field. We call it consistent formulation because no simplification is made in the computation of stress resultants other than the assumption of linear elastic material. Material stiffness coefficients of the laminate are integrated numerically without any approximation in the shifter. A displacement finite element model is derived with C^0-continuous elements. Higher-order p levels are used in interpolating the displacement field to preclude any effect of membrane and shear locking. Finally, numerical examples are presented to assess the accuracy of the present formulation when compared to the first-order shear deformation shell theory for isotropic and composite cylinders.

Shell Theory

Preliminaries

In this section, we will briefly discuss the mathematical preliminaries of the shell theory. The whole general tensor notation used here can be found in Refs. 8 and 32–35. Figure 1 shows the undeformed state of an arbitrary shell continuum. Let V be the volume of the undeformed (reference) configuration. Let S^+ and S^- denote the top and the bottom surfaces of the volume V and Ω be the undeformed midsurface of the shell such that

$$V = \Omega \times (-h/2, h/2) \tag{1}$$

The point P in V (surface $\bar{\Omega}$) is defined by a set of convected curvilinear coordinates, θ^1, θ^2 and θ^3, attached to the shell body and the point P_0 in Ω by θ^1 and θ^2, where θ^3 is the normal coordinate. Covariant and contravariant base vectors at P_0 in Ω are denoted by $\boldsymbol{a}_\alpha, \boldsymbol{a}^\alpha$ with metric $a_{\alpha\beta}, a^{\alpha\beta}$. We also define a normal vector to the midsurface $\boldsymbol{a}_3 = \boldsymbol{a}^3$ such that $\boldsymbol{a}_3 \cdot \boldsymbol{a}_3 = 1$. As usual, the Einstein summation convention is applied to repeated indices of tensor components where Greek indices represent the numbers 1 and 2 and Latin indices the numbers 1–3. Then

$$a_{\alpha\beta} = \boldsymbol{a}_\alpha \cdot \boldsymbol{a}_\beta, \qquad \boldsymbol{a}^{\alpha\beta} = \boldsymbol{a}^\alpha \cdot \boldsymbol{a}^\beta, \qquad \boldsymbol{a}^\alpha \cdot \boldsymbol{a}_\beta = \delta^\alpha_\beta$$

$$\boldsymbol{a}_\alpha \cdot \boldsymbol{a}_3 = 0, \qquad \boldsymbol{a}_\alpha = \frac{\partial \boldsymbol{r}}{\partial \theta^\alpha} = \boldsymbol{r}_{,\alpha}, \qquad \boldsymbol{r} = \boldsymbol{r}(\theta^1, \theta^2) \tag{2}$$

where $\boldsymbol{r}$ is the position vector of the point P_0 in Ω and δ^α_β is the mixed Kronecker delta function. The components of the metric tensor $a_{\alpha\beta}$ are known as the first fundamental form of the surface. In the following developments, $(),_i$ denotes partial derivatives with respect to the corresponding space coordinate, whereas $()_{\|i}$ and $()_{|\alpha}$ designate covariant derivatives with respect to space and surface metrics, respectively. In a similar fashion, covariant and contravariant base vectors at points of V are denoted by $\boldsymbol{g}_i, \boldsymbol{g}^i$ with corresponding metrics g_{ij}, g^{ij}. Thus,

$$g_{ij} = \boldsymbol{g}_i \cdot \boldsymbol{g}_j, \qquad g^{ij} = \boldsymbol{g}^i \cdot \boldsymbol{g}^j, \qquad \boldsymbol{g}^i \cdot \boldsymbol{g}_j = \delta^i_j$$

$$\boldsymbol{g}_i = \frac{\partial \boldsymbol{R}}{\partial \theta^i} = \boldsymbol{R}_{,i}, \qquad \boldsymbol{R} = \boldsymbol{R}(\theta^1, \theta^2, \theta^3) \tag{3}$$

where $\boldsymbol{R}$ is the position vector of a typical point P in V (Fig. 1).

The description of the three-dimensional shell continuum can be obtained by expressing the position vector $\boldsymbol{R}$ at the point P in terms of $\boldsymbol{r}$ and the unit vector $\boldsymbol{a}_3$. Namely,

$$\boldsymbol{R} = \boldsymbol{r} + \theta^3 \boldsymbol{a}_3 \tag{4}$$

In view of Eq. (4), the covariant vectors $\boldsymbol{g}_\alpha$ and $\boldsymbol{a}_\alpha$ are related according to the expression

$$\boldsymbol{g}_\alpha = \boldsymbol{a}_\alpha + \theta^3 \boldsymbol{a}_{3,\alpha}, \qquad \boldsymbol{g}_3 = \boldsymbol{a}_3 \tag{5}$$

It follows that

$$g_{\alpha 3} = g^{\alpha 3} = 0, \qquad g_{33} = g^{33} = 1 \tag{6}$$

The covariant components of the curvature tensor (second fundamental form of the surface) are defined by

$$b_{\alpha\beta} = \boldsymbol{r}_{,\alpha\beta} \cdot \boldsymbol{a}_3 = \boldsymbol{a}_{\alpha,\beta} \cdot \boldsymbol{a}_3 = -\boldsymbol{a}_\alpha \cdot \boldsymbol{a}_{3,\beta} \tag{7}$$

and the mixed components of the curvature tensor by

$$b^\alpha_\beta = a^{\alpha\mu} b_{\mu\beta} \tag{8}$$

We also define the components of the third fundamental form of the surface as

$$c_{\alpha\beta} = b^\lambda_\alpha b_{\lambda\beta} \tag{9}$$

By means of the well-known Weingarten formula

$$\boldsymbol{a}_{3,\alpha} = -b^\lambda_\alpha \boldsymbol{a}_\lambda \tag{10}$$

the first equation of expression (5) can be transformed into

$$\boldsymbol{g}_\alpha = \mu^\beta_\alpha \boldsymbol{a}_\beta, \qquad \mu^\beta_\alpha = \delta^\beta_\alpha - \theta^3 b^\beta_\alpha \tag{11}$$

with μ^β_α as the shifter tensor components of the shell continuum.

The following additional definitions and relationships are needed in the sequel

$$a = \det(a_{\alpha\beta}), \qquad g = \det(g_{ij}), \qquad \mu = \det\left(\mu^\beta_\alpha\right)$$

$$\mu = \sqrt{g/a} = 1 - 2H\theta^3 + K(\theta^3)^2 \tag{12}$$

where H and K, respectively, denote the mean and Gaussian curvatures of the surface.

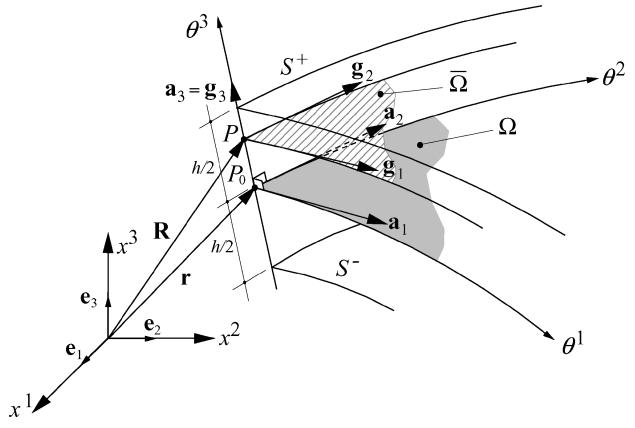

Fig. 1 Undeformed state of arbitrary shell continuum.

Kinematics of Deformation of Shells

Let $\boldsymbol{v}$ be the displacement vector associated with a point P in V. It can be expressed either in terms of the space base vectors $\boldsymbol{g}_i$ (or $\boldsymbol{g}^i$) in V or the surface base vectors $\boldsymbol{a}_\alpha$ and $\boldsymbol{a}_3$ in Ω. Namely,

$$\boldsymbol{v} = V^i \boldsymbol{g}_i = V_i \boldsymbol{g}^i = v^\alpha \boldsymbol{a}_\alpha + v^3 \boldsymbol{a}_3 = v_\alpha \boldsymbol{a}^\alpha + v_3 \boldsymbol{a}^3 \tag{13}$$

where (V^i, V_i) and (v^i, v_i) are the contravariant and covariant components of the vector $\boldsymbol{v}$ in V and Ω, respectively.

Similarly, the Green–Lagrange strain tensor $\boldsymbol{E}$ can be expressed in terms of the space or surface base vectors. Then

$$\boldsymbol{E} = E_{ij}\boldsymbol{g}^i \otimes \boldsymbol{g}^j = \bar{E}_{ij}\boldsymbol{a}^i \otimes \boldsymbol{a}^j \tag{14}$$

where E_{ij} and $\bar{E}_{ij}$ are the covariant components of the tensor $\boldsymbol{E}$. The tensor components E_{ij} measure the difference of metrics between the deformed and undeformed configurations. It can be shown that

$$E_{ij} = \tfrac{1}{2}(\boldsymbol{g}_i \cdot \boldsymbol{v}_{,j} + \boldsymbol{g}_j \cdot \boldsymbol{v}_{,i} + \underline{\boldsymbol{v}_{,i} \cdot \boldsymbol{v}_{,j}}) = \tfrac{1}{2}\big(V_{i\|j} + V_{j\|i} + \underline{V^k_{\|i} V_{k\|j}}\big) \tag{15}$$

Because we are dealing here with the small deformation shell theory, the underlined terms of Eq. (15) may be dropped. Then, the linear strain components are

$$\varepsilon_{ij} = \tfrac{1}{2}(V_{i\|j} + V_{j\|i}) \tag{16}$$

The space and surface components of the displacement vector are connected by the following equations:

$$V_\alpha = \mu^\beta_\alpha v_\beta, \qquad V_3 = v_3 \tag{17}$$

and the covariant derivatives of a vector $\boldsymbol{v}$ in V are related to its covariant derivatives in Ω according to the following expression[33,34]:

$$V_{\alpha\|\beta} = \mu^\lambda_\alpha(v_{\lambda|\beta} - b_{\lambda\beta}v_3), \qquad V_{\alpha\|3} = \mu^\lambda_\alpha v_{\lambda,3}$$
$$V_{3\|\alpha} = v_{3,\alpha} + b^\lambda_\alpha v_\lambda, \qquad V_{3\|3} = v_{3,3} \tag{18}$$

Equation (16) can be written as

$$\varepsilon_{\alpha\beta} = \tfrac{1}{2}(V_{\alpha\|\beta} + V_{\beta\|\alpha}), \qquad \varepsilon_{\alpha3} = \tfrac{1}{2}(V_{\alpha\|3} + V_{3\|\alpha}), \qquad \varepsilon_{33} = V_{3\|3} \tag{19}$$

Finally, substituting expression (18) into Eq. (19), we obtain the exact strain–displacement relations of the shell,

$$\begin{aligned}
\varepsilon_{\alpha\beta} &= \tfrac{1}{2}\big[\mu^\lambda_\alpha(v_{\lambda|\beta} - b_{\lambda\beta}v_3) + \mu^\lambda_\beta(v_{\lambda|\alpha} - b_{\lambda\alpha}v_3)\big] \\
&= \big[\tfrac{1}{2}(v_{\alpha|\beta} + v_{\beta|\alpha}) - b_{\alpha\beta}v_3\big] + \big[c_{\alpha\beta}v_3 - \tfrac{1}{2}\big(b^\lambda_\alpha v_{\lambda|\beta} + b^\lambda_\beta v_{\lambda|\alpha}\big)\big](\theta^3) \\
\varepsilon_{\alpha3} &= \tfrac{1}{2}\big(\mu^\lambda_\alpha v_{\lambda,3} + v_{3,\alpha} + b^\lambda_\alpha v_\lambda\big) \\
&= \tfrac{1}{2}\big(v_{\alpha,3} + v_{3,\alpha} + b^\lambda_\alpha v_\lambda\big) + \tfrac{1}{2}\big(-b^\lambda_\alpha v_{\lambda,3}\big)(\theta^3) \\
\varepsilon_{33} &= v_{3,3}
\end{aligned} \tag{20}$$

Next, we introduce the following assumptions to derive the present formulation:

1) The displacement field considered is based on a cubic expansion of the thickness coordinate around the midsurface, and the transverse displacement is assumed to be constant through the thickness.

2) Fourth- or higher-order terms in the strain–displacement relations of the shell are neglected.

3) The normal stresses perpendicular to the midsurface are neglected.

The first two are kinematic assumptions, whereas the last one is commonly used[6] in shell theories. Assumption 1 was originally proposed in papers by Reddy[11] and Reddy and Liu,[12] where a nine-parameter formulation obtained initially is reduced to a five-parameter one imposing the tangential traction-free conditions on S^+ and S^-. In addition, the second part of assumption 1 asserts the unstretched condition of the material line normal to the midsurface. Then, the displacement field can be written as

$$v_\alpha(\theta^i) = u_\alpha + \varphi_\alpha\theta^3 + \gamma_\alpha(\theta^3)^2 + \eta_\alpha(\theta^3)^3, \qquad v_3(\theta^i) = u_3 \tag{21}$$

The stress tensor $\boldsymbol{\sigma}$ and the stress vector $\boldsymbol{t}$ can be expressed in terms of the covariant space vectors $\boldsymbol{g}_i$ as

$$\boldsymbol{\sigma} = \sigma^{ij}\boldsymbol{g}_i \otimes \boldsymbol{g}_j, \qquad \boldsymbol{t} = t^\alpha \boldsymbol{g}_\alpha + t^3\boldsymbol{g}_3 \tag{22}$$

The absence of tangential tractions on S^+ and S^- implies that $t^\alpha = 0$. Using the Cauchy formula on the top and bottom surfaces with $\boldsymbol{n} = \boldsymbol{g}_3$ and $-\boldsymbol{g}_3$, respectively, we arrive at the following condition:

$$t^\alpha = \sigma^{3\alpha}|_{S^+,S^-} = 0 \tag{23}$$

Note that for anisotropic materials the generalized Hooke's law is written as

$$\sigma^{ij} = E^{ijkl}\varepsilon_{kl} \tag{24}$$

where E^{ijkl} are contravariant space components of the elasticity tensor associated with a linear elastic body. Substituting Eq. (24) into condition (23), and considering that the material is orthotropic, we arrive at the final expression for condition (23),

$$\varepsilon_{3\alpha}|_{S^+,S^-} = 0 \tag{25}$$

The displacement field (21) substituted into the second of Eqs. (20) and expression (25), gives

$$\begin{aligned}
\gamma_\alpha &= -\tfrac{1}{3}b^\lambda_\alpha(d^{-1})^\beta_\lambda\big(\varphi_\beta + u_{3,\beta} + b^\kappa_\beta u_\kappa\big) \\
\eta_\alpha &= -(4/3h^2)(d^{-1})^\beta_\alpha\big(\varphi_\beta + u_{3,\beta} + b^\kappa_\beta u_\kappa\big)
\end{aligned} \tag{26}$$

where $(d^{-1})^\beta_\alpha$ is the inverse of d^β_α and is defined as

$$(d^{-1})^\lambda_\alpha d^\beta_\lambda = \delta^\beta_\alpha \qquad d^\alpha_\beta = \delta^\alpha_\beta[1 - (h^2/12)K] - (h^2/6)b^\alpha_\beta H \tag{27}$$

When Eq. (26) is taken into account, the displacement field (21) can now be written as

$$v_\alpha(\theta^i) = u_\alpha + \varphi_\alpha\theta^3 + \underline{h^\lambda_\alpha(d^{-1})^\beta_\lambda\big(\varphi_\beta + u_{3,\beta} + b^\kappa_\beta u_\kappa\big)}$$
$$v_3(\theta^i) = u_3 \tag{28}$$

where

$$h^\beta_\alpha = \big[-\tfrac{1}{3}b^\beta_\alpha(\theta^3)^2 - (4/3h^2)\delta^\beta_\alpha(\theta^3)^3\big] \tag{29}$$

The nine-parameter theory given by Eq. (21) is now reduced to a five-parameter one (with variables u_i and φ_α), which has the same number of variables as the first-order shell theory.[8,33] The present first-order shear deformation theory (FSDT) can be obtained from Eq. (28) neglecting the underlined terms and is also known as the Reissner–Mindlin theory. Substituting Eq. (28) into the strain–displacement equations given in Eq. (20), we obtain the following relations:

$$\varepsilon_{\alpha\beta} = \varepsilon^{(0)}_{\alpha\beta} + \varepsilon^{(1)}_{\alpha\beta}(\theta^3) + \varepsilon^{(2)}_{\alpha\beta}(\theta^3)^2 + \varepsilon^{(3)}_{\alpha\beta}(\theta^3)^3 + \underline{\varepsilon^{(4)}_{\alpha\beta}(\theta^3)^4}$$
$$\varepsilon_{\alpha3} = \varepsilon^{(0)}_{\alpha3} + \varepsilon^{(1)}_{\alpha3}(\theta^3) + \varepsilon^{(2)}_{\alpha3}(\theta^3)^2 + \varepsilon^{(3)}_{\alpha3}(\theta^3)^3, \qquad \varepsilon_{33} = 0 \tag{30}$$

where the underlined term is neglected by assumption 2.

Assumption 3 implies the normal stress is zero. However, the second part of assumption 1 states the strain component $\varepsilon_{33} = 0$ in evident contradiction to the constitutive equations. A justification for these assumptions can be found by Koiter.[36] Shell formulations that include a linear variation of the thickness stretch have been proposed by Büchter and Ramm[37] and Simo et al.[38]

Finally, the coefficients $\varepsilon^{(i)}_{\alpha\beta}$ and $\varepsilon^{(i)}_{\alpha3}$ of Eq. (30) are given by

$$\begin{aligned}
\varepsilon^{(0)}_{\alpha\beta} &= \tfrac{1}{2}(u_{\alpha|\beta} + u_{\beta|\alpha}) - b_{\alpha\beta}u_3 \\
\varepsilon^{(1)}_{\alpha\beta} &= \tfrac{1}{2}\big(\varphi_{\alpha|\beta} + \varphi_{\beta|\alpha} - b^\lambda_\alpha u_{\lambda|\beta} - b^\lambda_\beta u_{\lambda|\alpha}\big) + c_{\alpha\beta}u_3 \\
\varepsilon^{(2)}_{\alpha\beta} &= \tfrac{1}{2}\big(\gamma_{\alpha|\beta} + \gamma_{\beta|\alpha} - b^\lambda_\alpha\varphi_{\lambda|\beta} - b^\lambda_\beta\varphi_{\lambda|\alpha}\big) \\
\varepsilon^{(3)}_{\alpha\beta} &= \tfrac{1}{2}\big(\eta_{\alpha|\beta} + \eta_{\beta|\alpha} - b^\lambda_\alpha\gamma_{\lambda|\beta} - b^\lambda_\beta\gamma_{\lambda|\alpha}\big) \\
\varepsilon^{(4)}_{\alpha\beta} &= \tfrac{1}{2}\big(-b^\lambda_\alpha\eta_{\lambda|\beta} - b^\lambda_\beta\eta_{\lambda|\alpha}\big), \qquad \varepsilon^{(0)}_{\alpha3} = \tfrac{1}{2}\big(\varphi_\alpha + u_{3,\alpha} + b^\lambda_\alpha u_\lambda\big) \\
\varepsilon^{(1)}_{\alpha3} &= \gamma_\alpha, \qquad \varepsilon^{(2)}_{\alpha3} = \tfrac{1}{2}\big(3\eta_\alpha - b^\lambda_\alpha\gamma_\lambda\big), \qquad \varepsilon^{(3)}_{\alpha3} = -b^\lambda_\alpha\eta_\lambda
\end{aligned} \tag{31}$$

where γ_α and η_α are defined in Eq. (26).

Constitutive Equations

Consider a composite shell built of a finite number N of laminas, which are made of an arbitrary linear elastic orthotropic material. It is also assumed that the layers are perfectly bonded together without any slip among their interfaces. The principal material axes are allowed to be oriented differently from layer to layer. At each point of the layer L $(L = 1, N)$, we set a local orthogonal coordinate system $\bar{\theta}^\alpha$ such that the corresponding base vectors $\bar{\boldsymbol{g}}_\alpha$ coincide at P with the principal material directions and are, furthermore, of unit length. The third coordinate $\theta^3 = \bar{\theta}^3$ remains unchanged. The constitutive equations with respect to this system are given by

$$\bar{\sigma}^{ij} = \bar{E}_L^{ijkl}\bar{\varepsilon}_{kl} \tag{32}$$

where $\bar{E}_L^{mnkl}$ are the tensor components of the elasticity tensor referred to $\bar{\theta}^i$ and identical at P with the physical ones (because $\bar{\boldsymbol{g}}_i$ are orthonormal basis). Therefore, these coefficients can be calculated in terms of the engineering elastic constants, which can be found in several textbooks of composite materials.[39]

The transformation of Eq. (32) to the laminate coordinates θ^i gives

$$\sigma^{ij} = E_L^{ijkl}\varepsilon_{kl} \tag{33}$$

where

$$E_L^{ijkl} = \frac{\partial\theta^i}{\partial\bar{\theta}^m}\frac{\partial\theta^j}{\partial\bar{\theta}^n}\frac{\partial\theta^k}{\partial\bar{\theta}^p}\frac{\partial\theta^l}{\partial\bar{\theta}^q}\bar{E}_L^{mnpq} \tag{34}$$

The base vectors in coordinates $\bar{\theta}^i$ and θ^i are related by

$$\bar{\boldsymbol{g}}_m = \frac{\partial\theta^j}{\partial\bar{\theta}^m}\boldsymbol{g}_j \tag{35}$$

which implies

$$E_L^{ijkl} = (\boldsymbol{g}^i\cdot\bar{\boldsymbol{g}}_m)(\boldsymbol{g}^j\cdot\bar{\boldsymbol{g}}_n)(\boldsymbol{g}^k\cdot\bar{\boldsymbol{g}}_p)(\boldsymbol{g}^l\cdot\bar{\boldsymbol{g}}_q)\bar{E}_L^{mnpq} \tag{36}$$

Finally, we use assumption 3 of zero stress condition in the thickness direction. This leads to

$$\sigma^{\alpha\beta} = C_L^{\alpha\beta\omega\rho}\varepsilon_{\omega\rho}, \qquad \sigma^{\alpha 3} = 2C_L^{\alpha 3\omega 3}\varepsilon_{\omega 3} \tag{37}$$

with the reduced elasticity tensor

$$C_L^{\alpha\beta\omega\rho} = E_L^{\alpha\beta\omega\rho} - E_L^{\alpha\beta 33}\left(E_L^{33\omega\rho}\big/E_L^{3333}\right), \qquad C_L^{\alpha 3\omega 3} = E_L^{\alpha 3\omega 3} \tag{38}$$

Principle of Virtual Work and Stress Resultants

For the displacement finite element formulation, the virtual work principle of the laminated continuum is utilized. It asserts that "If a continuum body is in equilibrium then the virtual work of the total forces is zero under a virtual displacement"[40] and is expressed in terms of the stress and strain tensor as

$$\delta W = \delta W_I + \delta W_E = \int_V \sigma^{ij}\delta\varepsilon_{ij}\,\mathrm{d}V + \int_\Omega P^j\delta V_j\,\mathrm{d}\Omega = 0 \tag{39}$$

where δW_I is the virtual work of the internal forces, δW_E the virtual work of external forces, and δ is the variational operator. Because the integration is carried out over the undeformed configuration, the volume element is given by

$$\mathrm{d}V = \sqrt{g}\,\mathrm{d}\theta^1\,\mathrm{d}\theta^2\,\mathrm{d}\theta^3 = \mu\,\mathrm{d}\Omega\,\mathrm{d}\theta^3 \tag{40}$$

where g and μ are related by Eq. (12). The surface element is defined by

$$\mathrm{d}\Omega = \sqrt{a}\,\mathrm{d}\theta^1\,\mathrm{d}\theta^2 \tag{41}$$

Substituting Eq. (40) into the expression of the internal virtual work, we obtain

$$\delta W_I = \int_V \mu\sigma^{ij}\delta\varepsilon_{ij}\,\mathrm{d}\Omega\,\mathrm{d}\theta^3 \tag{42}$$

The decisive step in the definition of stress resultants is to split expression (42) into a surface integral and an integral in the transverse direction using relations (31). Furthermore, in view of the condition $\varepsilon_{33} = 0$, we obtain

$$\delta W_I = \int_V \left(\sigma^{\alpha\beta}\sum_{n=0}^{3}(\theta^3)^{(n)}\delta\varepsilon_{\alpha\beta}^{(n)} + 2\sigma^{\alpha 3}\sum_{n=0}^{3}(\theta^3)^{(n)}\delta\varepsilon_{\alpha 3}^{(n)}\right)\mu\,\mathrm{d}\Omega\,\mathrm{d}\theta^3 \tag{43}$$

The preintegration along the thickness through the laminate leads to a two-dimensional virtual work principle,

$$\delta W = \int_\Omega \left(\sum_{n=0}^{3}\overset{(n)}{N}{}^{\alpha\beta}\,\delta\varepsilon_{\alpha\beta}^{(n)} + 2\sum_{n=0}^{3}\overset{(n)}{Q}{}^{\alpha 3}\,\delta\varepsilon_{\alpha 3}^{(n)}\right)\mathrm{d}\Omega + \int_\Omega P^j\delta V_j\,\mathrm{d}\Omega = 0 \tag{44}$$

The stress resultants $\overset{(n)}{N}{}^{\alpha\beta}$ and $\overset{(n)}{Q}{}^{\alpha 3}$ are given by

$$\overset{(n)}{N}{}^{\alpha\beta} = \int_{-h/2}^{h/2}\mu\sigma^{\alpha\beta}(\theta^3)^n\,\mathrm{d}\theta^3$$

$$\overset{(n)}{Q}{}^{\alpha 3} = \int_{-h/2}^{h/2}\mu\sigma^{\alpha 3}(\theta^3)^n\,\mathrm{d}\theta^3, \qquad n = 0, 1, 2, 3 \tag{45}$$

The scalar quantity μ, which is the determinant of the shell shifter tensor, contains information about changes of differential geometry, that is, the size and the shape of a differential volume element throughout the shell thickness. We can now expand expression (45) by using Eq. (37) with Eq. (30):

$$\overset{(n)}{N}{}^{\alpha\beta} = \int_{-h/2}^{h/2}\mu\sigma^{\alpha\beta}(\theta^3)^n\,\mathrm{d}\theta^3 = \sum_{L=1}^{N}\int_{h_L}^{h_{L+1}}\mu C_L^{\alpha\beta\omega\rho}\times\left[\sum_{k=0}^{3}(\theta^3)^k\varepsilon_{\omega\rho}^{(k)}\right](\theta^3)^n\,\mathrm{d}\theta^3 = \sum_{k=0}^{3}\overset{k+n}{C}{}^{\alpha\beta\omega\rho}\,\varepsilon_{\omega\rho}^{(k)}, \qquad n = 0, 1, 2, 3 \tag{46}$$

$$\overset{(n)}{Q}{}^{\alpha 3} = \int_{-h/2}^{h/2}\mu\sigma^{\alpha 3}(\theta^3)^n\,\mathrm{d}\theta^3 = 2\sum_{L=1}^{N}\int_{h_L}^{h_{L+1}}\mu C_L^{\alpha 3\beta 3}\times\left[\sum_{k=0}^{3}(\theta^3)^k\varepsilon_{\beta 3}^{(k)}\right](\theta^3)^n\,\mathrm{d}\theta^3 = 2\sum_{k=0}^{3}\overset{k+n}{C}{}^{\alpha 3\beta 3}\,\varepsilon_{\beta 3}^{(k)}, \qquad n = 0, 1, 2, 3 \tag{47}$$

where material stiffness coefficients of the laminate are given by

$$\overset{k}{C}{}^{\alpha\beta\omega\rho} = \sum_{L=1}^{N}\left(\int_{h_L}^{h_{L+1}}\mu C_L^{\alpha\beta\omega\rho}(\theta^3)^k\,\mathrm{d}\theta^3\right)$$

$$\overset{k}{C}{}^{\alpha 3\beta 3} = \sum_{L=1}^{N}\left(\int_{h_L}^{h_{L+1}}\mu C_L^{\alpha 3\beta 3}(\theta^3)^k\,\mathrm{d}\theta^3\right), \qquad k = 0, 1, \ldots, 6 \tag{48}$$

Integration shown in Eq. (48) of the material law through the thickness direction is fundamental in reducing the three-dimensional theory to the two-dimension one. The actual process of calculation of Eq. (48) is carried out numerically using the Gaussian integration formula with at least 10 Gauss points per layer.

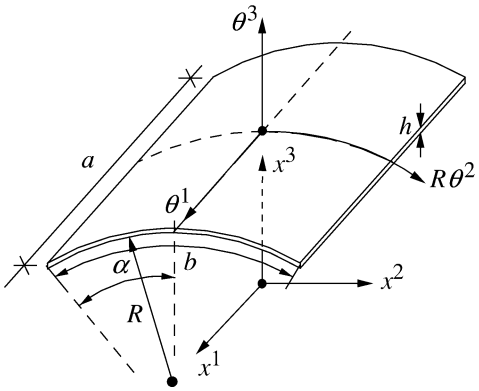

Fig. 2 Circular cylindrical shell geometry.

Finite Element Implementation

Mathematical Model

Let the geometry of a cylindrical panel be defined by Fig. 2, where θ^i, $i = 1, 2, 3$, are curvilinear coordinates of the shell placed at the center of the midsurface. Let x^i, $i = 1, 2, 3$, be a set of rectangular Cartesian coordinates defining a three-dimensional Euclidean space with base vectors $\boldsymbol{e}_i$. The midsurface Ω of the shell is described by the vector $\boldsymbol{r}$ such that

$$\boldsymbol{r} = \boldsymbol{r}(x^i) = x^i \boldsymbol{e}_i \tag{49}$$

where $x^i = x^i(\theta^\alpha)$. These components are

$$x^1 = \theta^1, \qquad x^2 = (R + \theta^3)\sin(\theta^2), \qquad x^3 = (R + \theta^3)\cos(\theta^2) \tag{50}$$

For circular cylindrical geometry, the following quantities can be obtained:

$$\begin{gathered} a_{11} = 1, \qquad a_{22} = R^2, \qquad a_{12} = a_{21} = 0 \\ a^{11} = 1, \qquad a^{22} = 1/R^2, \qquad a^{12} = a^{21} = 0 \\ b_{11} = 0, \qquad b_{22} = -R, \qquad b_{12} = b_{21} = 0, \qquad b_1^1 = 0 \\ b_2^2 = -1/R, \qquad b_2^1 = b_1^2 = 0 \\ \mu_1^1 = 1, \qquad \mu_2^2 = 1 + \theta^3/R, \qquad \mu_2^1 = \mu_1^2 = 0 \end{gathered} \tag{51}$$

and the space metric tensor components g_{ij} (referred to V) are

$$\begin{gathered} g_{11} = 1, \qquad g_{22} = (R + \theta^3)^2, \qquad g_{12} = g_{21} = 0 \\ g_{23} = g_{13} = 0, \qquad g_{33} = 1 \end{gathered} \tag{52}$$

Let f_i and F_{ij} be space components of a vector and a tensor, respectively, in orthogonal basis. Their physical components are then defined by[34]

$$\begin{gathered} f_{\langle i\rangle} = \sqrt{g_{ii}}\, f^i = \sqrt{g^{ii}}\, f_i \\ F_{\langle ij\rangle} = \sqrt{g_{ii} g_{jj}}\, F^{ij} = \sqrt{g^{ii} g^{jj}}\, F_{ij} \qquad \text{(no sum)} \end{gathered} \tag{53}$$

Thus, the following equations are obtained:

$$\begin{gathered} \sigma_{\langle 11\rangle} = \sigma^{11}, \qquad \sigma_{\langle 22\rangle} = (R+\theta^3)^2\sigma^{22}, \qquad \sigma_{\langle 12\rangle} = (R+\theta^3)\sigma^{12} \\ \sigma_{\langle 13\rangle} = \sigma^{13}, \qquad \sigma_{\langle 23\rangle} = (R+\theta^3)\sigma^{23} \\ \varepsilon_{\langle 11\rangle} = \varepsilon_{11}, \qquad \varepsilon_{\langle 22\rangle} = \varepsilon_{22}\big/(R+\theta^3)^2, \qquad \varepsilon_{\langle 12\rangle} = \varepsilon_{12}\big/(R+\theta^3) \\ \varepsilon_{\langle 13\rangle} = \varepsilon_{13}, \qquad \varepsilon_{\langle 23\rangle} = \varepsilon_{23}\big/(R+\theta^3) \\ v_{\langle 1\rangle} = v_1, \qquad v_{\langle 2\rangle} = v_2/R, \qquad v_{\langle 3\rangle} = v_3 \end{gathered} \tag{54}$$

After the substitution of quantities (51) and (54) into Eqs. (31), the explicit kinematics for cylindrical shells can be derived. Details of these expressions for the third-order shear theory and the first-order shear theory are given in the Appendix for brevity.

Finite Element Discretization

This section is devoted to the development of the displacement finite element model for laminate shells based on the principle of virtual work. It is well known[10] that this kind of model requires the use of Lagrange interpolation functions for all generalized displacements (C^0 element) for the FSDT. On the other hand, because of the presence of first partial derivatives of the variable u_3 in the displacement field equations (28), the finite element model for the third-order shear deformation theory (TSDT) requires Hermite interpolation for the transverse deflection (C^1 element) and Lagrange interpolation for other displacements.

It has been shown that finite element models for shells based on C^1-continuity elements are numerically inconvenient because they involve second partial derivatives of the interpolation functions and cannot account for all rigid-body modes of a curved element.[22] Furthermore, the C^1-continuity element can be used only for mapping rectangular meshes not distorted ones because the constant curvature criterion could be violated.[21] Therefore, it is desirable to impose on the displacement field a C^0 continuity with polynomials of equal degree to overcome these problems.

For this reason, we relax the continuity in the displacement field by using the following auxiliary variables:

$$\psi_\alpha = \varphi_\alpha + u_{3,\alpha} \tag{55}$$

which were already used by Nayak et al.[25] for composite plates. Substituting Eq. (55) in Eq. (28), we have

$$v_\alpha(\theta^i) = u_\alpha + \varphi_\alpha\theta^3 + h_\alpha^\lambda (d^{-1})_\lambda^\beta \left(\psi_\beta + b_\beta^\kappa u_\kappa\right), \qquad v_3(\theta^i) = u_3 \tag{56}$$

which requires only C^0 continuity in all primary variables. Equation (56) is now used to obtain the new kinematic relations of the shell and, hence, the variational formulation for the finite element model. As a result of Eq. (56), the number of variables to be interpolated is seven for the TSDT and five for the FSDT.

The finite element equations are obtained by discretizing the physical components of displacements and rotations. Then

$$\begin{gathered} u_{\langle 1\rangle} = \sum_{j=1}^{m} u_{(j)} N_{(j)}(\theta^1, \theta^2), \qquad u_{\langle 2\rangle} = \sum_{j=1}^{m} v_{(j)} N_{(j)}(\theta^1, \theta^2) \\ u_{\langle 3\rangle} = \sum_{j=1}^{m} w_{(j)} N_{(j)}(\theta^1, \theta^2) \\ \varphi_{\langle 1\rangle} = \sum_{j=1}^{m} \varphi_{(j)}^1 N_{(j)}(\theta^1, \theta^2), \qquad \varphi_{\langle 2\rangle} = \sum_{j=1}^{m} \varphi_{(j)}^2 N_{(j)}(\theta^1, \theta^2) \\ \psi_{\langle 1\rangle} = \sum_{j=1}^{m} \psi_{(j)}^1 N_{(j)}(\theta^1, \theta^2), \qquad \psi_{\langle 2\rangle} = \sum_{j=1}^{m} \psi_{(j)}^2 N_{(j)}(\theta^1, \theta^2) \end{gathered} \tag{57}$$

where m is the number of nodes of the element, $N_{(j)}(\theta^1, \theta^2)$ is the Lagrange interpolation function at the node j, and $(u_{(j)}, v_{(j)}, w_{(j)}, \varphi_{(j)}^1, \varphi_{(j)}^2, \psi_{(j)}^1, \psi_{(j)}^2)$ are the nodal values of the displacements. The Lagrange polynomials are given by

$$\begin{gathered} L_i^1(\xi) = \prod_{\substack{k=1 \\ k\neq i}}^{p+1} \frac{(\xi - \xi_k)}{(\xi_i - \xi_k)}, \qquad L_i^2(\eta) = \prod_{\substack{k=1 \\ k\neq i}}^{p+1} \frac{(\eta - \eta_k)}{(\eta_i - \eta_k)} \\ i = 1, \ldots, p+1 \end{gathered} \tag{58}$$

where p is the polynomial degree. Finally, the shape function mapped in the biunit square is of the form

$$N_{\langle k\rangle} = L_i^1(\xi) L_j^2(\eta), \qquad k = (j-1)(p+1) + i \tag{59}$$

Finite elements based on these interpolation functions are known to have locking problems due to inconsistencies in the modeling of transverse shear energy and membrane energy. The locking is avoided in many cases by using uniformly reduced integration in

Table 1 Number of degrees of freedom (DOF) per element for different p levels

Element	p level	FSDT (DOF)	TSDT (DOF)
$Q4$	1	20	28
$Q9$	2	45	63
$Q25$	4	125	175
$Q49$	6	245	343
$Q81$	8	405	567

Table 2 Numerical integration rule for different p levels used in present formulation

p level	Full integration	Selective integration	Reduced integration
1	$2\times2\times2$	$2\times1\times1$	$1\times1\times1$
2	$3\times3\times3$	$3\times2\times2$	$2\times2\times2$
4	$5\times5\times5$	$5\times4\times4$	$4\times4\times4$
6	$7\times7\times7$	$7\times6\times6$	$6\times6\times6$
8	$9\times9\times9$	$9\times8\times8$	$8\times8\times8$

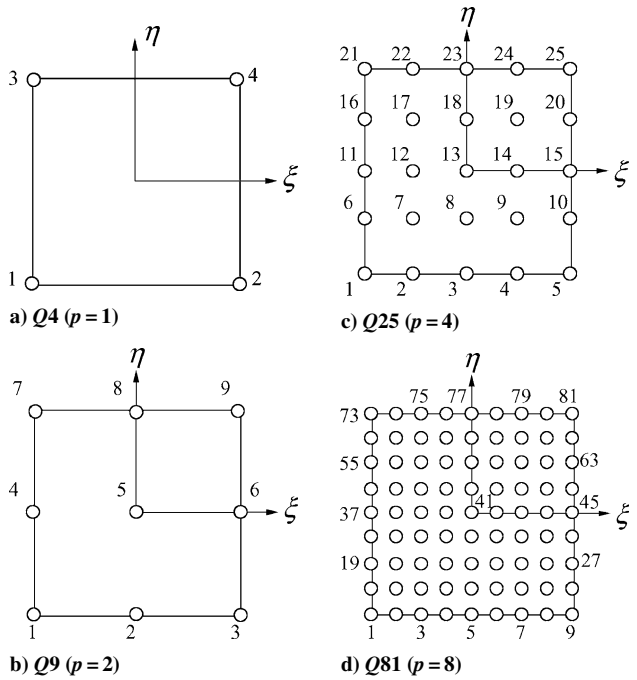

Fig. 3 Basic p elements used in present formulation.

the numerical evaluation of stiffness coefficients. In other cases, selective integration proves to be more accurate. Pontaza and Reddy[31] used higher-order spectral interpolation plate elements to avoid shear locking. Following the same idea, a family of higher-order Lagrange elements has been developed to overcome this deficiency (Fig. 3). For comparison reasons, reduced and selective integration techniques have also been implemented. Table 1 shows the family of higher-order Lagrange elements utilized in this paper and the corresponding number of degrees of freedom for the FSDT and TSDT, whereas Fig. 4 shows the shape function N_8 associated with the element $Q25$.

The numerical integration rule (Gauss quadrature) used in the present formulation is shown in Table 2, where the last number denotes the number of Gauss points used to evaluate transverse shear terms, that is, those related to $\varepsilon^{(i)}_{\alpha 3}$ the middle one denotes the number of Gauss points used to evaluate the bending-membrane coupling terms (related to $\varepsilon^{(0)}_{22}$ and $\varepsilon^{(1)}_{22}$), and the first one denotes the number of Gauss points used to evaluate the remaining terms in the stiffness matrix. The code allows using full integration for all terms, reduced integration (one point less than full integration) for all terms, or selective integration in which reduced integration is used for both shear and bending-membrane terms and full integration for all other terms.

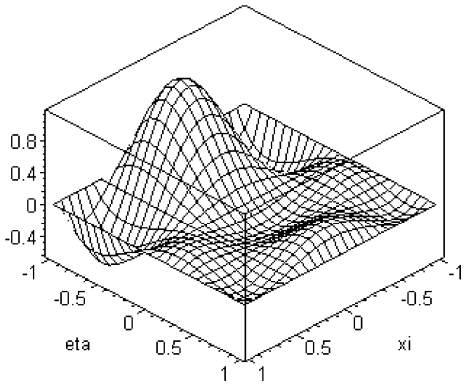

Fig. 4 Interpolation function N_8 for $Q25$ element ($p = 4$).

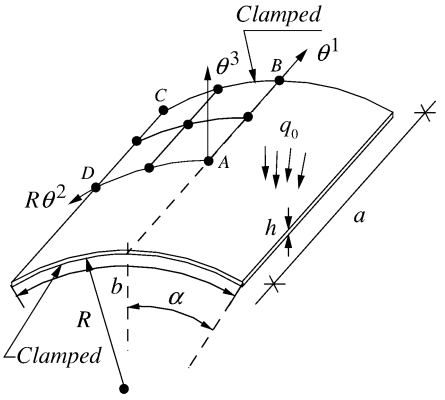

Fig. 5 Clamped cylindrical shell panel with uniformly transverse load.

Numerical Results

In this section are presented some numerical examples obtained with the formulation developed herein. The performance of the developed element and the TSDT formulation is evaluated by solving several benchmark problems. First, three well-known isotropic shell problems are analyzed, and then a composite shell panel with closed-form solution previously reported is examined.

Clamped Shallow Panel

The first problem to be considered is a clamped shallow panel under pressure load.[41] This problem exhibits strong shear locking (where ratio $R/h = 800$). Because of the symmetry of the problem, a quarter of the full panel is considered as the computational domain (Fig. 5). The geometric and material data for the problem are

$$E = 0.45\times10^6 \text{ psi}, \qquad \nu = 0.3, \qquad a = 20 \text{ in.}$$
$$R = 100 \text{ in.}, \qquad h = 0.125 \text{ in.}, \qquad \alpha = 0.1 \text{ rad} \qquad (60)$$

The panel is subjected to uniform transverse load $q_0 = 0.04$ psi with the following boundary conditions.

At $\theta^1 = 0$ (symmetry):

$$u_{\langle 1\rangle} = \varphi_{\langle 1\rangle} = \psi_{\langle 1\rangle} = 0$$

At $\theta^2 = 0$ (symmetry):

$$u_{\langle 2\rangle} = \varphi_{\langle 2\rangle} = \psi_{\langle 2\rangle} = 0$$

At $\theta^1 = a/2$ and $\theta^2 = \alpha$:

$$u_{\langle 1\rangle} = u_{\langle 2\rangle} = u_{\langle 3\rangle} = \varphi_{\langle 1\rangle} = \varphi_{\langle 2\rangle} = \psi_{\langle 1\rangle} = \psi_{\langle 2\rangle} = 0$$

Two sets of uniform meshes are used in the analysis (one with 81 nodes and other with 289 nodes). The vertical displacement at the center of the shell obtained with various p levels and integration rules is presented in Table 3 for the TSDT as well as the FSDT. For this problem, Palazotto and Dennis[41] reported a vertical deflection at the center as 0.01144 in. and Brebbia and Connor[42] reported

Table 3 Vertical deflection at center of clamped cylindrical panel ($-u_{\langle 3\rangle} \times 10^2$ in.) under uniformly transverse load

	Mesh of 81 nodes			Mesh of 289 nodes		
p level	Full integration	Selective integration	Reduced integration	Full integration	Selective integration	Reduced integration
1						
TSDT	0.294404	1.156251	1.157727	0.690335	1.140095	1.140459
FSDT	0.337791	1.156233	1.157720	0.745615	1.140085	1.140457
2						
TSDT	1.172442	1.135172	1.135228	1.142842	1.134908	1.134908
FSDT	1.172160	1.135157	1.135219	1.142721	1.134901	1.134906
4						
TSDT	1.134782	1.134897	1.134896	1.134892	1.134894	1.134892
FSDT	1.134775	1.134888	1.134885	1.134888	1.134889	1.134890
8						
TSDT	1.134895	1.134883	1.134889	1.134892	1.134892	1.134893
FSDT	1.134888	1.134878	1.134876	1.134890	1.134889	1.134889

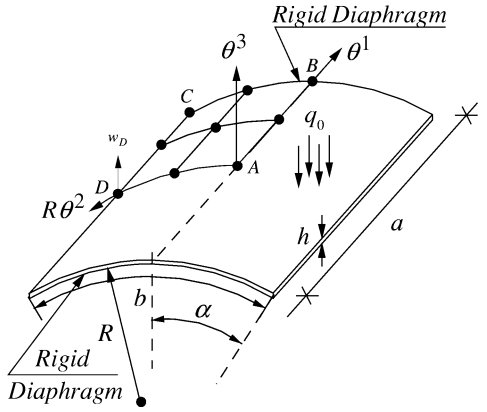

Fig. 6 Barrel vault benchmark with deadweight load.

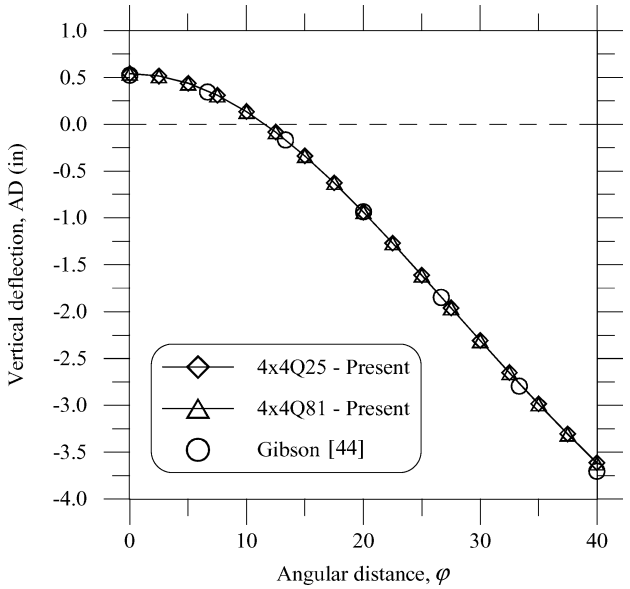

Fig. 7 Vertical deflection of the curve *AD* in the barrel vault.

0.011 in. The results obtained for the $Q4$ element with full integration show the presence of strong shear locking. Selective or reduced integrations for these cases are, in general, in good agreement with those cited before. However, they tend to overestimate deflections. On the other hand, high-order elements ($Q25$ and $Q81$) perform very well under strong shear locking and give excellent results using full integration.

Barrel Vault

This benchmark is also well known as the Scordelis–Lo roof (Fig. 6). The first authors to present a solution for this problem appear to be Cantin and Clough[22] (using $\nu = 0.3$ instead to zero). They compared their results with those obtained by the Scordelis and Lo[43] program for cylindrical shallow shells. An analytical solution was obtained by Gibson,[44] who reported the vertical displacement at the center of the free edge as 3.70331 in. (Also see Ashwell.[45]) For a deep shell, other authors give a value of 3.6288 in. for the vertical deflection.[7] We adopt the latter result as the referent solution for this example (w_{ref}). The geometric and material data for the problem are the following:

$$E = 3 \times 10^6 \text{ psi}, \qquad \nu = 0$$

$$a = 600 \text{ in.}, \qquad R = 300 \text{ in.}, \qquad h = 3 \text{ in.}, \qquad \alpha = 0.6981 \text{ rad} \tag{61}$$

The deadweight loading can be expressed in components θ^2 as

$$P^2 = q_0 \sin(\theta^2), \qquad P^3 = -q_0 \cos(\theta^2) \tag{62}$$

where $q_0 = 0.625$ psi. Finally, the boundary conditions on the computational domain are as follows.

At $\theta^1 = 0$ (symmetry):

$$u_{\langle 1\rangle} = \varphi_{\langle 1\rangle} = \psi_{\langle 1\rangle} = 0$$

At $\theta^2 = 0$ (symmetry):

$$u_{\langle 2\rangle} = \varphi_{\langle 2\rangle} = \psi_{\langle 2\rangle} = 0$$

At $\theta^1 = a/2$:

$$u_{\langle 2\rangle} = u_{\langle 3\rangle} = \phi_{\langle 2\rangle} = 0$$

Here, we are considering the free edge at $\theta^2 = \alpha$.

The vertical deflection at point D for uniform meshes of 289 nodes and 1089 nodes with different p levels is reported in Table 4. The analysis is carried out for the TSDT and FSDT with various integration rules. It is clearly shown that shear and membrane locking is avoided by using higher-order p level elements ($Q25$ and $Q81$). Again, the results obtained with selective and reduced integration are in close agreement with those with meshes of $4 \times 4 Q25$ and $4 \times 4 Q81$ with full integration.

The vertical deflection of the line AD and axial displacement of the line BC are shown in Figs. 7 and 8 and compared with those of Gibson.[44]

To illustrate the performance of the elements $Q25$ and $Q81$, in Fig. 9 is shown the convergence analysis of the vertical deflection at the center of the free edge for different p levels (all results for the TSDT). We note that an excellent rate of convergence is achieved if higher-order elements are employed.

Pinched Cylinder

Another known isotropic benchmark for cylindrical shell is the pinched cylinder with end diaphragms shown in Fig. 10. This has

Table 4 Vertical deflection at center of free edge ($-w_D$ in.) of barrel vault

	Mesh of 289 nodes			Mesh of 1089 nodes		
p level	Full integration	Selective integration	Reduced integration	Full integration	Selective integration	Reduced integration
1						
TSDT	0.838487	3.247487	3.622260	1.726715	3.517603	3.620960
FSDT	0.897689	3.247861	3.618373	1.830634	3.517676	3.617874
2						
TSDT	3.591876	3.613964	3.622168	3.611742	3.617631	3.620785
FSDT	3.591688	3.614232	3.617881	3.611326	3.617452	3.617682
4						
TSDT	3.612094	3.617789	3.622350	3.615259	3.618267	3.620811
FSDT	3.611798	3.617730	3.617731	3.614648	3.617669	3.617670
8						
TSDT	3.614360	3.618341	3.622618	3.617565	3.618798	3.620846
FSDT	3.613857	3.617779	3.617780	3.616582	3.617669	3.617670

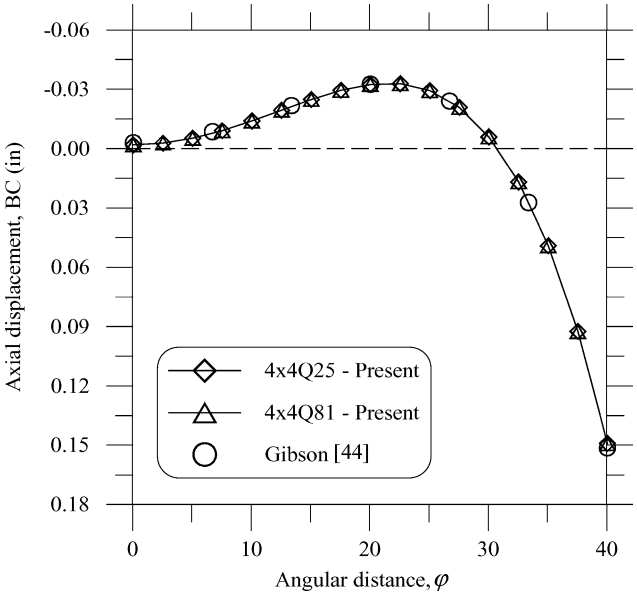

Fig. 8 Axial displacement $u_{\langle 1\rangle}$ of curve BC in barrel vault.

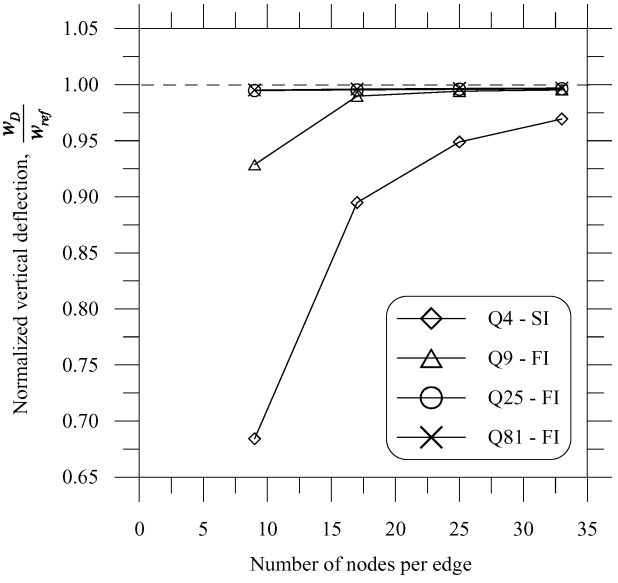

Fig. 9 Convergence of vertical deflection w_D at center of free edge of barrel vault.

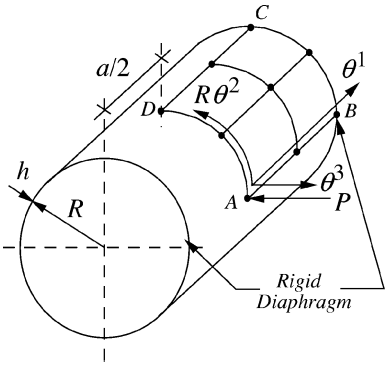

Fig. 10 Geometry of pinched circular cylinder with end diaphragms.

been used by many researchers and is identified as one of the most severe tests for both inextensional bending and complex membrane states. The pinched shell is supported at each end by a rigid diaphragm and loaded by two opposed forces acting at midpoint of the shell. Because of the symmetry condition of the structure, an octant of the cylinder is considered as the computational domain. The following geometrical data and material properties are used:

$$E = 3 \times 10^6 \text{ psi}, \qquad \nu = 0.3, \qquad a = 600 \text{ in.}$$

$$R = 300 \text{ in.}, \qquad h = 3 \text{ in.}, \qquad \alpha = \pi/2 \text{ rad} \tag{63}$$

with load $P = 1.0$ lb and the following boundary conditions.

At $\theta^1 = 0$ (symmetry):

$$u_{\langle 1\rangle} = \varphi_{\langle 1\rangle} = \psi_{\langle 1\rangle} = 0$$

At $\theta^2 = 0, \alpha$ (symmetry):

$$u_{\langle 2\rangle} = \varphi_{\langle 2\rangle} = \psi_{\langle 2\rangle} = 0$$

At $\theta^1 = a/2$:

$$u_{\langle 2\rangle} = u_{\langle 3\rangle} = \varphi_{\langle 2\rangle} = 0$$

In Table 5, we present results for the displacement at the point A with meshes of 289 nodes and 1089 nodes and different p levels. The analytical solution given by Flügge[46] is -1.8248×10^{-5} in. However, because Flügge neglected the shear deformation (classical shell theory) in contrast with the present formulation, we adopt as the reference solution, w_{ref}, the value reported by Cho and Roh,[4] which is -1.8541×10^{-5} in. It is observed that the rate of convergence is slower than those obtained for the barrel vault. The results for $Q4$ and $Q9$ elements with full integration are far from the reference solution cited before, even using meshes with 1089 nodes. Yet we see very good convergence ratios for the $Q25$ and $Q81$ elements. In all cases, selective and reduced integrations overestimate the displacement at the point load.

Table 5 Radial displacement at A ($-u_{\langle 3\rangle} \times 10^5$ in.) of pinched cylinder

	Mesh of 289 nodes			Mesh of 1089 nodes		
p level	Full integration	Selective integration	Reduced integration	Full integration	Selective integration	Reduced integration
1						
TSDT	0.251812	1.774684	1.858685	0.550182	1.840790	1.866632
FSDT	0.278551	1.779810	1.861183	0.601829	1.846633	1.870120
2						
TSDT	1.216584	1.836614	1.858427	1.678857	1.859622	1.865619
FSDT	1.224521	1.841271	1.860786	1.685528	1.864953	1.868865
4						
TSDT	1.755459	1.848284	1.857482	1.832276	1.861194	1.864758
FSDT	1.758577	1.852522	1.859767	1.834672	1.866060	1.867858
8						
TSDT	1.831581	1.852502	1.856828	1.846517	1.862194	1.864251
FSDT	1.833630	1.856177	1.859076	1.848246	1.866501	1.867271

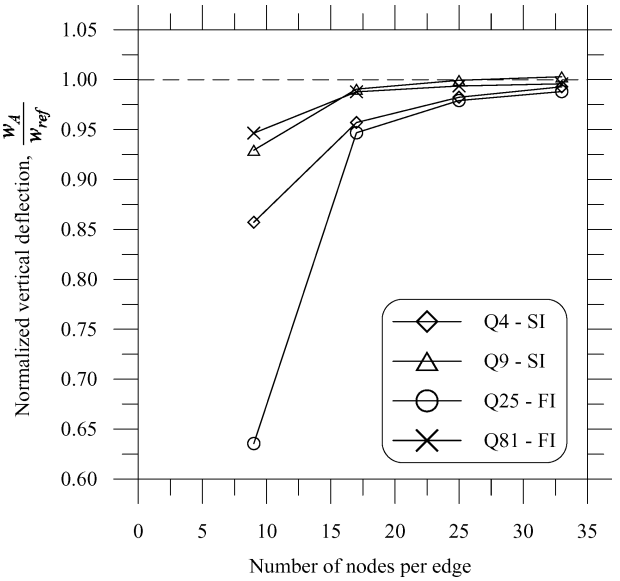

Fig. 11 Convergence of radial displacement $u_{\langle 3\rangle}$ at point A of pinched cylinder.

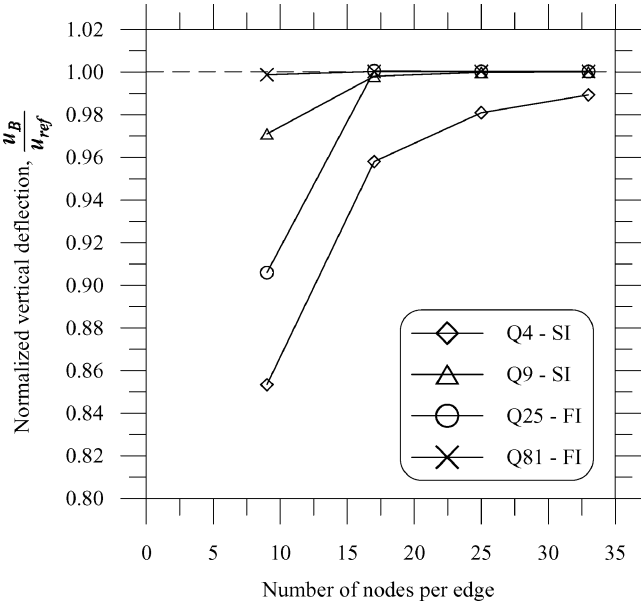

Fig. 12 Convergence of axial displacement u_B of pinched cylinder.

Figures 11 and 12 show a convergence study for the radial displacement at the point A and the axial displacement u_B (where $u_{\text{ref}} = -4.5711 \times 10^{-7}$ in.) using different p levels and elements. Again, all results are obtained using the TSDT. In both cases, the locking is overcome by using higher-order elements. Also note that the convergence of the axial displacement u_B is faster than w_A.

Finally, Fig. 13 shows a comparison between the radial deflection distribution of the line DC with meshes of $4 \times 4Q25$ and $4 \times 4Q81$ for the present TSDT formulation and the 8-URI (eight nodes with uniformly reduced integration) given by Kreja et al.[47] This particular example can be treated as the most severe one for the problem considered and is rarely noted in the literature.[48] We note that full integration with high p levels gives, in general, excellent results, minimizing the membrane and shear locking. The result reported for the displacement w_D is 5.22×10^{-8} in. (Ref. 48). All results suggest using at least meshes of 4×4 with $Q25$ elements to avoid locking.

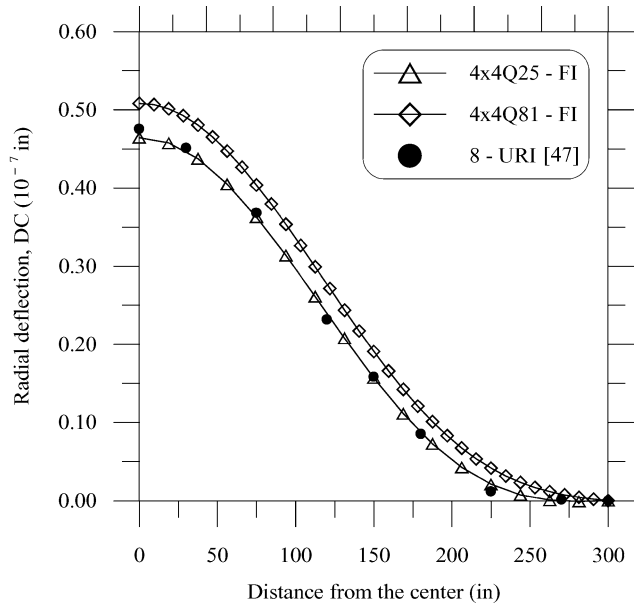

Fig. 13 Radial displacement distribution of line DC of pinched cylinder.

Circular Cylindrical Laminated Shell

Bending of a laminated cylindrical shell is studied. The model considered is a simply supported cross-ply cylinder under internal sinusoidal pressure. The problem was solved analytically by Varadan and Bhaskar[16] with the three-dimensional elasticity theory. Because of symmetry conditions, a panel of length a, angle 2α, and radius R is analyzed considering simply supported boundary conditions at edges $\theta^1 = 0, a$ and $\theta^2 = 0, 2\alpha$. The dimensionless

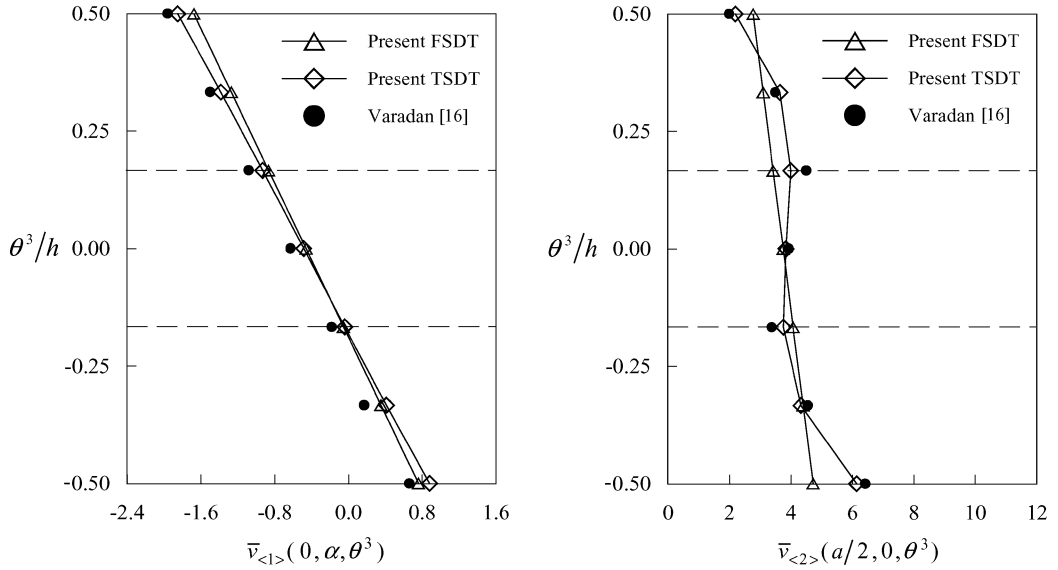

Fig. 14 Displacement distribution through the thickness $\bar{v}_{\langle 1\rangle}$ and $\bar{v}_{\langle 2\rangle}$ of three-ply (90/0/90 deg) laminated circular cylindrical panel ($4 \times 4Q25, S = 4$).

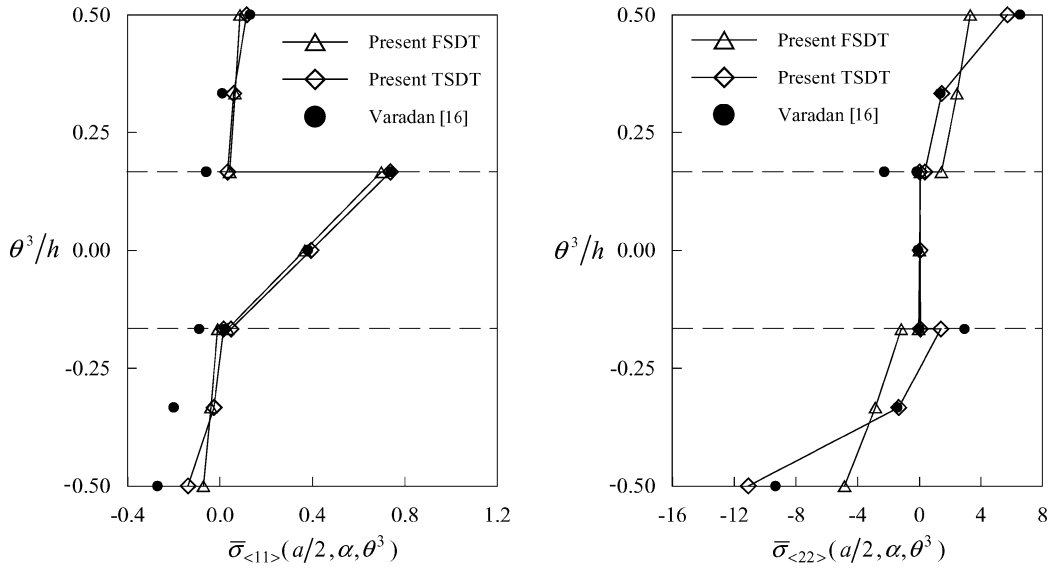

Fig. 15 Stress distribution through the thickness $\bar{\sigma}_{\langle 11\rangle}$ and $\bar{\sigma}_{\langle 22\rangle}$ of three-ply (90/0/90 deg) laminated circular cylindrical panel ($4 \times 4Q25, S = 4$).

material properties and geometrical data are the following:

$$E_1/E_2 = 25, \qquad G_{13} = G_{12} = 0.5E_2, \qquad G_{23} = 0.2E_2$$

$$\nu_{12} = 0.25, \qquad a/R = 4, \qquad R/h = S, \qquad \alpha = \pi/8 \quad (64)$$

The sinusoidal load can be expressed as

$$P^3 = q_0 \sin(\pi\theta^1/a)\sin(\pi\theta^2/2\alpha) \quad (65)$$

Because the effect of the laminate in bending response is unknown, the full panel is considered as the computational domain. The imposed simply supported boundary conditions are as follows.

At $\theta^1 = 0, a$:

$$u_{\langle 2\rangle} = u_{\langle 3\rangle} = \varphi_{\langle 2\rangle} = \psi_{\langle 2\rangle} = 0$$

At $\theta^2 = 0, 2\alpha$:

$$u_{\langle 1\rangle} = u_{\langle 3\rangle} = \varphi_{\langle 1\rangle} = \psi_{\langle 1\rangle} = 0$$

Tables 6–9 show results of the present FSDT and TSDT formulations compared with the three-dimensional analytical solutions of Varadan and Bhaskar[16] and the exact closed-form bending solutions of Cheng et al.[19] (for perfectly bonded layers). The results

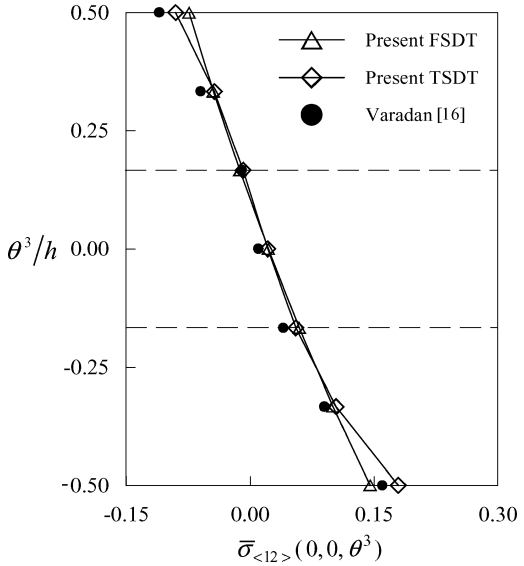

Fig. 16 Stress distribution through the thickness $\bar{\sigma}_{\langle 12\rangle}$ of three-ply (90/0/90 deg) laminated circular cylindrical panel ($4 \times 4Q25, S = 4$).

Table 6 Central deflection and stresses of single-ply (90 deg) laminated circular cylindrical panel under sinusoidal loading (4 × 4*Q*25 full integration)

S	Varadan and Bhaskar[16]	Present TSDT	Present FSDT
	$\bar{v}_{\langle 3\rangle}(a/2, \alpha, 0)$		
4	2.7830	2.98884	3.13878
10	0.9189	0.94796	0.94958
50	0.5385	0.54275	0.54262
100	0.5170	0.51883	0.51879
500	0.3060	0.30606	0.30606
	$\bar{\sigma}_{\langle 11\rangle}(a/2, \alpha, h/2)$		
4	0.0981	0.09229	0.07940
10	0.0663	0.06647	0.06112
50	0.0845	0.08500	0.08451
100	0.1190	0.11943	0.11924
500	0.2459	0.24640	0.24639
	$\bar{\sigma}_{\langle 11\rangle}(a/2, \alpha, -h/2)$		
4	−0.2295	−0.09150	−0.05780
10	−0.0656	−0.04530	−0.04021
50	−0.0086	−0.00791	−0.00795
100	0.0288	0.02905	0.02898
500	0.1924	0.19250	0.19249
	$\bar{\sigma}_{\langle 22\rangle}(a/2, \alpha, h/2)$		
4	4.8590	4.50830	3.12988
10	4.0510	4.17300	3.64722
50	3.9020	3.94390	3.89663
100	3.8430	3.87300	3.85435
500	2.3060	2.35160	2.34976
	$\bar{\sigma}_{\langle 22\rangle}(a/2, \alpha, -h/2)$		
4	−6.9690	−8.03680	−4.75957
10	−4.5090	−4.79990	−4.30457
50	−3.9790	−4.01090	−4.01432
100	−3.8760	−3.88490	−3.89186
500	−2.2930	−2.28300	−2.28437
	$\bar{\sigma}_{\langle 12\rangle}(0, 0, h/2)$		
4	−0.0925	−0.07165	−0.07330
10	−0.0436	−0.03910	−0.03745
50	−0.0243	−0.02379	−0.02362
100	−0.0161	−0.01586	−0.01579
500	0.0249	0.02498	0.02498
	$\bar{\sigma}_{\langle 12\rangle}(0, 0, -h/2)$		
4	0.0840	0.09652	0.09529
10	0.0412	0.04697	0.04570
50	0.0383	0.03929	0.03932
100	0.0447	0.04515	0.04518
500	0.0611	0.06110	0.06111

Table 7 Central deflection and stresses of two-ply (0/90 deg) laminated circular cylindrical panel under sinusoidal loading (4 × 4*Q*25 full integration)

S	Varadan and Bhaskar[16]	Cheng et al.[19]	Present TSDT	Present FSDT
	$\bar{v}_{\langle 3\rangle}(a/2, \alpha, 0)$			
4	6.1000	5.09696	6.66980	7.32821
10	3.3300	3.16576	3.44978	3.67150
50	2.2420	2.23717	2.26272	2.28648
100	1.3670	1.36665	1.37380	1.37812
500	0.1005	0.10049	0.10060	0.10061
	$\bar{\sigma}_{\langle 11\rangle}(a/2, \alpha, h/2)$			
4	0.2120	0.20710	0.24272	0.23042
10	0.1930	0.19098	0.20242	0.20389
50	0.2189	0.21866	0.22122	0.22223
100	0.1871	0.18708	0.18838	0.18860
500	0.0449	0.04491	0.04509	0.04508
	$\bar{\sigma}_{\langle 11\rangle}(a/2, \alpha, -h/2)$			
4	−0.9610	−0.71888	−0.93037	−0.90572
10	−0.1689	−0.15665	−0.17017	−0.17541
50	1.6100	1.60510	1.62290	1.63873
100	2.3000	2.29788	2.30920	2.31605
500	0.9436	0.94359	0.94424	0.94427
	$\bar{\sigma}_{\langle 22\rangle}(a/2, \alpha, h/2)$			
4	10.310	12.07122	12.57100	10.38730
10	10.590	10.95205	11.32900	10.92150
50	8.9370	8.95433	9.06240	9.02585
100	5.5600	5.56430	5.62630	5.60604
500	0.4345	0.43460	0.44868	0.44816
	$\bar{\sigma}_{\langle 22\rangle}(a/2, \alpha, -h/2)$			
4	−1.7890	−1.11616	−1.68620	−1.79515
10	−1.3430	−1.20498	−1.32470	−1.42100
50	−0.9670	−0.96152	−0.97207	−0.98588
100	−0.5759	−0.57495	−0.57771	−0.58073
500	−0.0339	−0.03392	−0.03428	−0.03430
	$\bar{\sigma}_{\langle 12\rangle}(0, 0, h/2)$			
4	−0.20070	−0.16858	−0.20324	−0.21694
10	−0.12470	−0.11819	−0.12606	−0.13019
50	0.07840	0.07842	0.07938	0.08080
100	0.18190	0.18187	0.18279	0.18354
500	0.09250	0.09245	0.09252	0.09253
	$\bar{\sigma}_{\langle 12\rangle}(0, 0, -h/2)$			
4	0.28120	0.22653	0.29249	0.32172
10	0.23250	0.22105	0.24039	0.25724
50	0.34490	0.34440	0.34835	0.35231
100	0.34520	0.34514	0.34690	0.34809
500	0.10450	0.10448	0.10457	0.10457

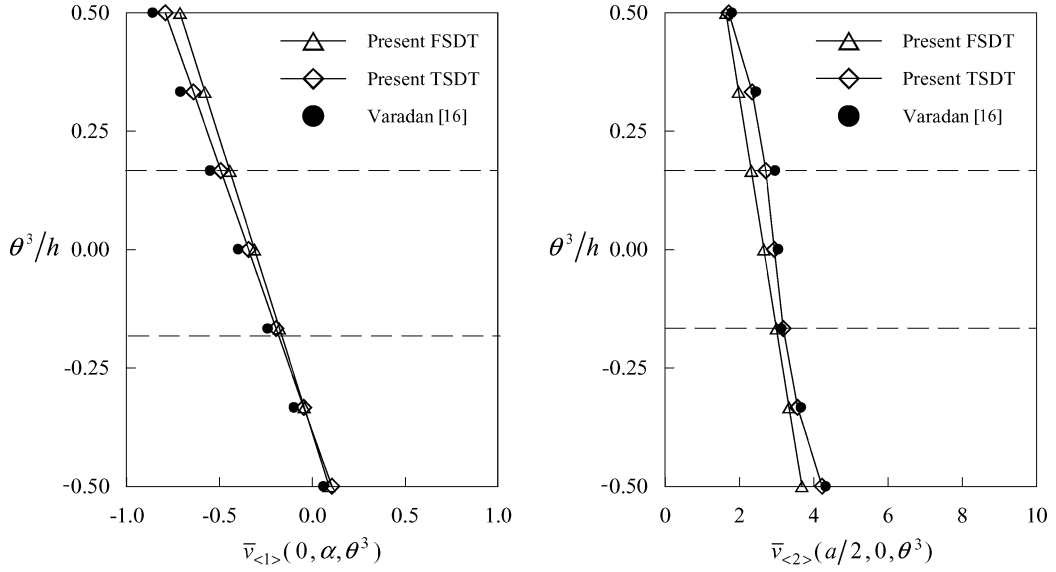

Fig. 17 Displacement distribution through the thickness $\bar{v}_{\langle 1\rangle}$ and $\bar{v}_{\langle 2\rangle}$ of three-ply (90/0/90 deg) laminated circular cylindrical panel (4 × 4*Q*25, *S* = 10).

Table 8 Central deflection and stresses of three-ply (90/0/90 deg) laminated circular cylindrical panel under sinusoidal loading (4 × 4*Q*25 full integration)

S	Varadan and Bhaskar[16]	Cheng et al.[19]	Present TSDT	Present FSDT
		$\bar{v}_{\langle 3\rangle}(a/2, \alpha, 0)$		
4	4.0090	3.60671	4.08163	3.79904
10	1.2230	1.20335	1.18349	1.07135
50	0.5495	0.54862	0.55044	0.54574
100	0.4715	0.47110	0.47273	0.47180
500	0.1027	0.10269	0.10280	0.10280
		$\bar{\sigma}_{\langle 11\rangle}(a/2, \alpha, h/2)$		
4	0.1270	0.12126	0.11545	0.08576
10	0.0739	0.07231	0.07156	0.06040
50	0.0712	0.07097	0.07147	0.07061
100	0.0838	0.08370	0.08414	0.08387
500	0.0559	0.05585	0.05604	0.05603
		$\bar{\sigma}_{\langle 11\rangle}(a/2, \alpha, -h/2)$		
4	−0.2701	−0.12923	−0.13848	−0.07216
10	−0.0791	−0.05632	−0.05790	−0.04695
50	−0.0225	−0.02167	−0.02192	−0.02189
100	0.0018	0.00197	0.00199	0.00191
500	0.0379	0.03788	0.03796	0.03795
		$\bar{\sigma}_{\langle 22\rangle}(a/2, \alpha, h/2)$		
4	6.5450	7.01022	5.72740	3.30200
10	4.6830	4.69967	4.66530	3.80004
50	3.9300	3.92646	3.96520	3.90776
100	3.5070	3.50478	3.53300	3.51579
500	0.7895	0.78973	0.80447	0.80400
		$\bar{\sigma}_{\langle 22\rangle}(a/2, \alpha, -h/2)$		
4	−9.3230	−10.5280	−11.08700	−4.84184
10	−5.2240	−5.30760	−5.46550	−4.41580
50	−3.9870	−3.98701	−4.01660	−3.99775
100	−3.5070	−3.50626	−3.51520	−3.51627
500	−0.7542	−0.75451	−0.74965	−0.75001
		$\bar{\sigma}_{\langle 12\rangle}(0, 0, h/2)$		
4	−0.1081	−0.08998	−0.09025	−0.07419
10	−0.0374	−0.03343	−0.03287	−0.02784
50	0.0118	0.01228	0.01225	0.01225
100	0.0478	0.04798	0.04812	0.04808
500	0.0766	0.07660	0.07665	0.07665
		$\bar{\sigma}_{\langle 12\rangle}(0, 0, -h/2)$		
4	0.1609	0.16242	0.17924	0.14534
10	0.0729	0.07569	0.07525	0.06597
50	0.0760	0.07639	0.07670	0.07613
100	0.1038	0.10393	0.10428	0.10412
500	0.0889	0.08886	0.08892	0.08892

Table 9 Central deflection and stresses of 10-ply $(90/0/90/0/90\ \text{deg})_s$ laminated circular cylindrical panel under sinusoidal loading (4 × 4*Q*25 full integration)

S	Varadan and Bhaskar[16]	Present TSDT	Present FSDT
		$\bar{v}_{\langle 3\rangle}(a/2, \alpha, 0)$	
4	4.2060	3.90209	4.18634
10	1.3800	1.31414	1.34037
50	0.7622	0.76468	0.76546
100	0.6261	0.62806	0.62820
500	0.1006	0.10067	0.10067
		$\bar{\sigma}_{\langle 11\rangle}(a/2, \alpha, h/2)$	
4	0.1243	0.11134	0.10011
10	0.0877	0.08637	0.08160
50	0.0971	0.09769	0.09719
100	0.1076	0.10812	0.10793
500	0.0516	0.05181	0.05180
		$\bar{\sigma}_{\langle 11\rangle}(a/2, \alpha, -h/2)$	
4	−0.2674	−0.12408	−0.09510
10	−0.0927	−0.07205	−0.06844
50	−0.0340	−0.03355	−0.03370
100	−0.0015	−0.00137	−0.00147
500	0.0340	0.03408	0.03408
		$\bar{\sigma}_{\langle 22\rangle}(a/2, \alpha, h/2)$	
4	6.6350	5.92790	4.66730
10	5.8750	5.97930	5.46968
50	5.5290	5.58740	5.53463
100	4.6770	4.71560	4.69626
500	0.7770	0.79232	0.79177
		$\bar{\sigma}_{\langle 22\rangle}(a/2, \alpha, -h/2)$	
4	−8.9700	−9.87600	−7.04297
10	−6.4620	−6.77990	−6.42938
50	−5.6060	−5.65260	−5.66983
100	−4.6700	−4.68270	−4.69327
500	−0.7351	−0.73172	−0.73215
		$\bar{\sigma}_{\langle 12\rangle}(0, 0, h/2)$	
4	0.0972	0.06956	0.07571
10	0.0406	0.03619	0.03508
50	−0.0223	−0.02273	−0.02297
100	−0.0734	−0.07373	−0.07382
500	−0.0829	−0.08298	−0.08298
		$\bar{\sigma}_{\langle 12\rangle}(0, 0, -h/2)$	
4	−0.1652	−0.15202	−0.16168
10	−0.0869	−0.08689	−0.08766
50	−0.1120	−0.11292	−0.11311
100	−0.1479	−0.14855	−0.14863
500	−0.0949	−0.09501	−0.09501

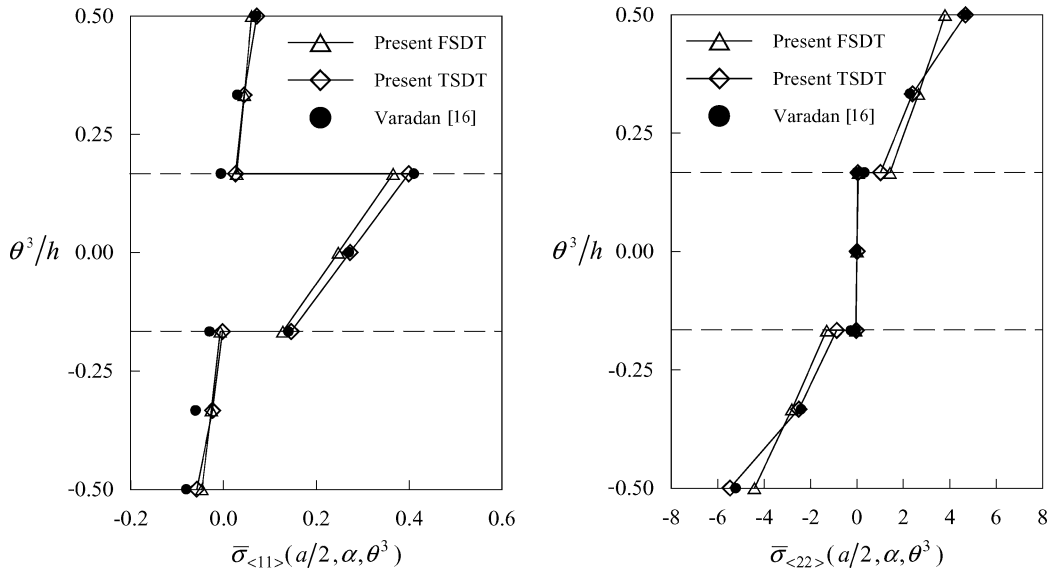

Fig. 18 Stress distribution through the thickness $\bar{\sigma}_{\langle 11\rangle}$ and $\bar{\sigma}_{\langle 22\rangle}$ of three-ply (90/0/90 deg) laminated circular cylindrical panel (4 × 4*Q*25, *S* = 10).

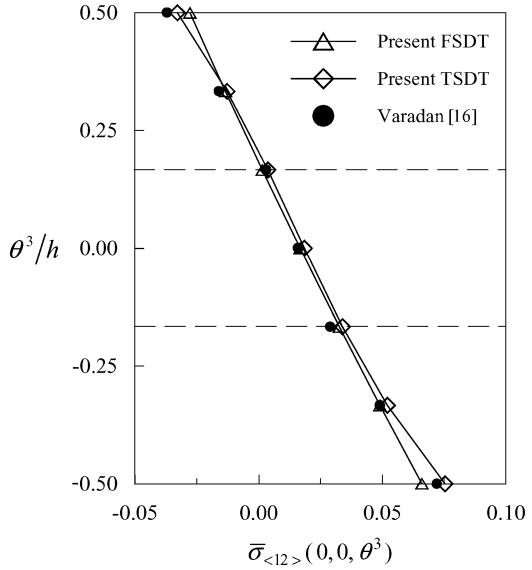

Fig. 19 Stress distribution through the thickness $\bar{\sigma}_{\langle 12\rangle}$ of three-ply (90/0/90 deg) laminated circular cylindrical panel ($4 \times 4Q25$, $S = 10$).

are tabulated for the dimensionless central deflection and stresses of cross-ply panels (four different kinds of laminates) and considering ratios $S = 4$, 10, 50, 100, and 500. The following quantities are introduced:

$$\bar{v}_{\langle\alpha\rangle} = \left(10E_1/q_0RS^2\right)v_{\langle\alpha\rangle}, \qquad \bar{v}_{\langle 3\rangle} = \left(10E_1/q_0RS^3\right)v_{\langle 3\rangle}$$

$$\bar{\sigma}_{\langle\alpha\beta\rangle} = \left(10/q_0S^2\right)\sigma_{\langle\alpha\beta\rangle}$$

A mesh of $4 \times 4Q25$ is used in the full panel, and the stiffness coefficients were evaluated using full integration. We observe that both theories give good results compared to the three-dimensional solutions. As we expected, these results diverge from the analytical solution when we have lower ratio S. In general, the TSDT appears to be more accurate than the FSDT, especially for thick shells.

Figures 14–22 show through the thickness distributions of in-surface displacements and bending stresses for the three-ply (90/0/90 deg) laminated shell for ratios $S = 4$, 10, and 100. Three theories, the present FSDT, the present TSDT, and the three-dimensional solutions of Varadan and Bhaskar[16] are compared. Again, we note a better performance of the TSDT over the FSDT (thickness distributions of displacements and stresses) for thick panels with $S = 4$ and 10, as clearly seen in Figs. 14 and 17.

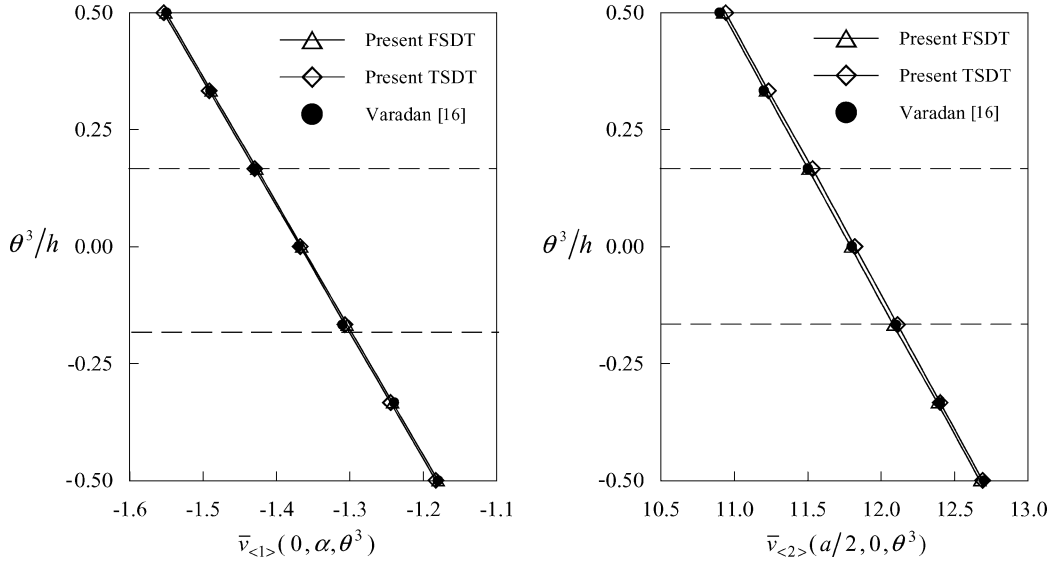

Fig. 20 Displacement distribution through the thickness $\bar{v}_{\langle 1\rangle}$ and $\bar{v}_{\langle 2\rangle}$ of three-ply (90/0/90 deg) laminated circular cylindrical panel ($4 \times 4Q25$, $S = 100$).

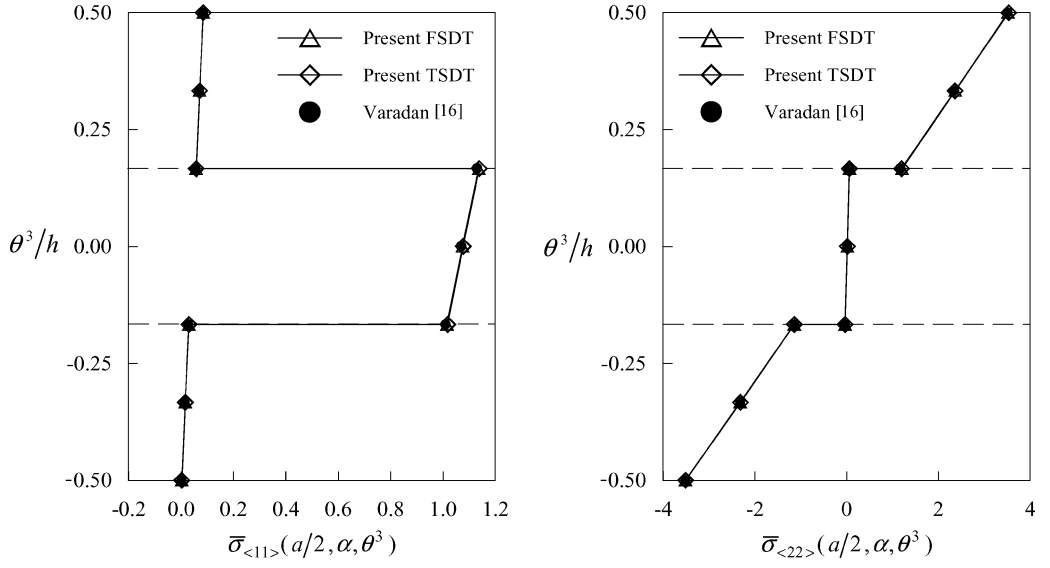

Fig. 21 Stress distribution through the thickness $\bar{\sigma}_{\langle 11\rangle}$ and $\bar{\sigma}_{\langle 22\rangle}$ of three-ply (90/0/90 deg) laminated circular cylindrical panel ($4 \times 4Q25$, $S = 100$).

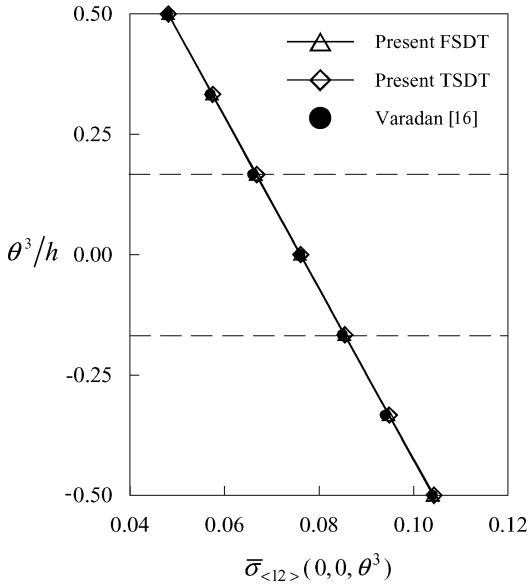

Fig. 22 Stress distribution through the thickness $\bar{\sigma}_{\langle 12\rangle}$ of three-ply (90/0/90 deg) laminated circular cylindrical panel ($4 \times 4Q25$, $S = 100$).

Conclusions

In the present study, a novel and consistent formulation of the TSDT for bending of composite shells is presented. The theory has seven independent variables. The FSDT included here is also novel in that it is consistently derived and is different from that of Naghdi. In both theories developed herein, no simplification is made in the computation of stress resultants and material stiffness coefficients of the laminate; they are integrated numerically without any approximation in the shifter. The displacement finite element model is derived with Lagrange elements with higher-order interpolation polynomials. Both formulations, the TSDT and FSDT, are found to be very accurate, as measured with the three-dimensional solutions found in the literature. The numerical results show that better performance is achieved by using the TSDT, in particular when dealing with thick shells. It is observed that the FSDT cannot reproduce as accurate displacement thickness distributions as the TSDT for shells with lower ratios S. By the use of higher-order p levels in interpolating the displacement field, effects of membrane and shear locking are minimized. In particular, it is found that $Q25$ and $Q81$ elements are strictly free of membrane and shear locking. The applicability of the refined TSDT in finite element analysis of shells has been demonstrated in this paper with a consistent mathematical framework and a straightforward finite element implementation.

Appendix: Kinematics of Cylindrical Shells

In this Appendix, the explicit form of the kinematics of circular cylindrical shells is presented. For convenience, we express the equations in terms of the physical components of the displacements. Based on Eqs. (53), we assert that

$$\varepsilon_{\langle ij\rangle} = \varepsilon_{ij}\Big/\sqrt{g_{ii}g_{jj}}, \qquad g_{ii} = \left(\mu_i^i\right)^2 a_{ii} \qquad \text{(no sum)} \quad \text{(A1)}$$

and then, we define $\bar{\varepsilon}_{\langle ij\rangle}$ as

$$\bar{\varepsilon}_{\langle ij\rangle} = \mu_i^i \mu_j^j \varepsilon_{\langle ij\rangle} = \varepsilon_{ij}\Big/\sqrt{a_{ii}a_{jj}} \qquad \text{(no sum)} \quad \text{(A2)}$$

FSDT

The strain field equations are

$$\bar{\varepsilon}_{\langle\alpha\beta\rangle} = \bar{\varepsilon}^{(0)}_{\langle\alpha\beta\rangle} + \bar{\varepsilon}^{(1)}_{\langle\alpha\beta\rangle}(\theta^3) + \underline{\bar{\varepsilon}^{(2)}_{\langle\alpha\beta\rangle}(\theta^3)^2}, \qquad \bar{\varepsilon}_{\langle\alpha 3\rangle} = \bar{\varepsilon}^{(0)}_{\langle\alpha 3\rangle} \quad \text{(A3)}$$

where the underlined term is neglected and

$$\bar{\varepsilon}^{(0)}_{\langle 11\rangle} = u_{\langle 1\rangle,1}, \qquad \bar{\varepsilon}^{(0)}_{\langle 22\rangle} = (1/R)u_{\langle 2\rangle,2} + u_{\langle 3\rangle}\Big/R$$

$$2\bar{\varepsilon}^{(0)}_{\langle 12\rangle} = (1/R)u_{\langle 1\rangle,2} + u_{\langle 2\rangle,1}, \qquad \bar{\varepsilon}^{(1)}_{\langle 11\rangle} = \varphi_{\langle 1\rangle,1}$$

$$\bar{\varepsilon}^{(1)}_{\langle 22\rangle} = (1/R)\varphi_{\langle 2\rangle,2} + \left(u_{\langle 2\rangle,2} + u_{\langle 3\rangle}\right)\Big/R^2$$

$$2\bar{\varepsilon}^{(1)}_{\langle 12\rangle} = \varphi_{\langle 1\rangle,2}\Big/R + \varphi_{\langle 2\rangle,1} + u_{\langle 2\rangle,1}\Big/R$$

$$\bar{\varepsilon}^{(2)}_{\langle 11\rangle} = 0, \qquad \bar{\varepsilon}^{(2)}_{\langle 22\rangle} = (1/R^2)\varphi_{\langle 2\rangle,2}$$

$$2\bar{\varepsilon}^{(2)}_{\langle 12\rangle} = (1/R)\varphi_{\langle 2\rangle,1}, \qquad 2\bar{\varepsilon}^{(0)}_{\langle 13\rangle} = \varphi_{\langle 1\rangle} + u_{\langle 3\rangle,1}$$

$$2\bar{\varepsilon}^{(0)}_{\langle 23\rangle} = \varphi_{\langle 2\rangle} + u_{\langle 3\rangle,2}\Big/R - u_{\langle 2\rangle}\Big/R \quad \text{(A4)}$$

TSDT

The strain–displacement equations are

$$\bar{\varepsilon}_{\langle\alpha\beta\rangle} = \bar{\varepsilon}^{(0)}_{\langle\alpha\beta\rangle} + \bar{\varepsilon}^{(1)}_{\langle\alpha\beta\rangle}(\theta^3) + \bar{\varepsilon}^{(2)}_{\langle\alpha\beta\rangle}(\theta^3)^2 + \bar{\varepsilon}^{(3)}_{\langle\alpha\beta\rangle}(\theta^3)^3 + \underline{\bar{\varepsilon}^{(4)}_{\langle\alpha\beta\rangle}(\theta^3)^4}$$

$$\bar{\varepsilon}_{\langle\alpha 3\rangle} = \bar{\varepsilon}^{(0)}_{\langle\alpha 3\rangle} + \bar{\varepsilon}^{(1)}_{\langle\alpha 3\rangle}(\theta^3) + \bar{\varepsilon}^{(2)}_{\langle\alpha 3\rangle}(\theta^3)^2 + \bar{\varepsilon}^{(3)}_{\langle\alpha 3\rangle}(\theta^3)^3 \quad \text{(A5)}$$

where the underlined term is neglected. We define the auxiliary functions as

$$\psi_{\langle 1\rangle} = \varphi_{\langle 1\rangle} + u_{\langle 3\rangle,1}, \qquad \psi_{\langle 2\rangle} = \varphi_{\langle 2\rangle} + (1/R)u_{\langle 3\rangle,2} \quad \text{(A6)}$$

Then the membrane strain components are

$$\bar{\varepsilon}^{(0)}_{\langle 11\rangle} = u_{\langle 1\rangle,1}, \qquad \bar{\varepsilon}^{(0)}_{\langle 22\rangle} = (1/R)u_{\langle 2\rangle,2} + u_{\langle 3\rangle}\Big/R$$

$$2\bar{\varepsilon}^{(0)}_{\langle 12\rangle} = (1/R)u_{\langle 1\rangle,2} + u_{\langle 2\rangle,1}, \qquad \bar{\varepsilon}^{(1)}_{\langle 11\rangle} = \varphi_{\langle 1\rangle,1}$$

$$\bar{\varepsilon}^{(1)}_{\langle 22\rangle} = (1/R)\varphi_{\langle 2\rangle,2} + \left(u_{\langle 2\rangle,2} + u_{\langle 3\rangle}\right)\Big/R^2$$

$$2\bar{\varepsilon}^{(1)}_{\langle 12\rangle} = \varphi_{\langle 1\rangle,2}\Big/R + \varphi_{\langle 2\rangle,1} + u_{\langle 2\rangle,1}\Big/R, \qquad \bar{\varepsilon}^{(2)}_{\langle 11\rangle} = 0$$

$$\bar{\varepsilon}^{(2)}_{\langle 22\rangle} = k_2\left[(1/R)\psi_{\langle 2\rangle,2} - u_{\langle 2\rangle,2}\Big/R^2\right] + (1/R^2)\varphi_{\langle 2\rangle,2}$$

$$2\bar{\varepsilon}^{(2)}_{\langle 12\rangle} = k_2\left(\psi_{\langle 2\rangle,1} - u_{\langle 2\rangle,1}\Big/R\right) + (1/R)\varphi_{\langle 2\rangle,1}, \qquad \bar{\varepsilon}^{(3)}_{\langle 11\rangle} = k_1\psi_{\langle 1\rangle,1}$$

$$\bar{\varepsilon}^{(3)}_{\langle 22\rangle} = k_3\left[(1/R)\psi_{\langle 2\rangle,2} - u_{\langle 2\rangle,2}\Big/R^2\right] + (k_2/R)\left[(1/R)\psi_{\langle 2\rangle,2} - u_{\langle 2\rangle,2}\Big/R^2\right]$$

$$2\bar{\varepsilon}^{(3)}_{\langle 12\rangle} = k_1\left(\psi_{\langle 1\rangle,2}\Big/R\right) + k_3\left(\psi_{\langle 2\rangle,1} - u_{\langle 2\rangle,1}\Big/R\right) + (k_2/R)\left(\psi_{\langle 2\rangle,1} - u_{\langle 2\rangle,1}\Big/R\right)$$

$$\bar{\varepsilon}^{(4)}_{\langle 11\rangle} = 0, \qquad \bar{\varepsilon}^{(4)}_{\langle 22\rangle} = (k_3/R)\left[(1/R)\psi_{\langle 2\rangle,2} - u_{\langle 2\rangle,2}\Big/R^2\right]$$

$$2\bar{\varepsilon}^{(4)}_{\langle 12\rangle} = (k_3/R)\left(\psi_{\langle 2\rangle,1} - u_{\langle 2\rangle,1}\Big/R\right) \quad \text{(A7a)}$$

and the shear strain components are

$$2\bar{\varepsilon}^{(0)}_{\langle 13\rangle} = \varphi_{\langle 1\rangle} + u_{\langle 3\rangle,1}$$

$$2\bar{\varepsilon}^{(0)}_{\langle 23\rangle} = \left[\varphi_{\langle 2\rangle} + (1/R)u_{\langle 3\rangle,2} - u_{\langle 2\rangle}\Big/R\right], \qquad \bar{\varepsilon}^{(1)}_{\langle 13\rangle} = 0$$

$$2\bar{\varepsilon}^{(1)}_{\langle 23\rangle} = 2k_2\left(\psi_{\langle 2\rangle} - u_{\langle 2\rangle}\Big/R\right), \qquad 2\bar{\varepsilon}^{(2)}_{\langle 13\rangle} = 3k_1\psi_{\langle 1\rangle}$$

$$2\bar{\varepsilon}^{(2)}_{\langle 23\rangle} = 3k_3\left(\psi_{\langle 2\rangle} - u_{\langle 2\rangle}\Big/R\right) + (k_2/R)\left(\psi_{\langle 2\rangle} - u_{\langle 2\rangle}\Big/R\right)$$

$$\bar{\varepsilon}^{(3)}_{\langle 13\rangle} = 0, \qquad 2\bar{\varepsilon}^{(3)}_{\langle 23\rangle} = (2k_3/R)\left(\psi_{\langle 2\rangle} - u_{\langle 2\rangle}\Big/R\right) \quad \text{(A7b)}$$

The constants k_1, k_2 and k_3 are given by

$$k_1 = -\frac{4}{3h^2}, \qquad k_2 = \frac{4R}{(12R^2 - h^2)}, \qquad k_3 = -\frac{16R^2}{(12R^2 - h^2)h^2} \tag{A8}$$

Acknowledgments

The authors acknowledge the support of the work by the U.S. Army Research Office through Grant DAAD19-01-1-0483. The second author gratefully acknowledges the support by the Oscar S. Wyatt Endowed professorship.

References

[1]Ahmad, S., Irons, B. M., and Zienkiewicz, O. C., "Analysis of Thick and Thin Shell Structures by Curved Finite Elements," *International Journal for Numerical Methods in Engineering*, Vol. 2, No. 3, 1970, pp. 419–451.

[2]Simo, J. C., and Fox, D. D., "On a Stress Resultant Geometrically Exact Shell Model. Part I: Formulation and Optimal Parametrization," *Computer Methods in Applied Mechanics and Engineering*, Vol. 72, No. 3, 1989, pp. 267–304.

[3]Chinosi, C., Della Croce, L., and Scapolla, T., "Hierarchic Finite Elements for Thin Naghdi Shell Model," *International Journal of Solids and Structures*, Vol. 35, No. 16, 1998, pp. 1863–1880.

[4]Cho, M., and Roh, H. Y., "Development of Geometrically Exact New Elements based on General Curvilinear Coordinates," *International Journal for Numerical Methods in Engineering*, Vol. 56, No. 1, 2003, pp. 81–115.

[5]Chapelle, D., Oliveira, D. L., and Bucalem, M. L., "MITC Elements for a Classical Shell Model," *Computers and Structures*, Vol. 81, No. 8–11, 2003, pp. 523–533.

[6]Büchter, N., and Ramm, E., "Shell Theory Versus Degeneration—A Comparison in Large Rotation Finite Element Analysis," *International Journal for Numerical Methods in Engineering*, Vol. 34, No. 1, 1992, pp. 39–59.

[7]Simo, J. C., Fox, D. D., and Rifai, M. S., "On a Stress Resultant Geometrically Exact Shell Model. Part II: The Linear Theory," *Computer Methods in Applied Mechanics and Engineering*, Vol. 73, No. 1, 1989, pp. 53–92.

[8]Naghdi, P. M., "Theory of Shells and Plates," *Handbuch der Physik*, Vol. VIa/2, Springer-Verlag, Berlin, 1972, pp. 425–640.

[9]Sansour, C., and Bednarczyk, H., "The Cosserat Surface as a Shell Model, Theory and Finite Element Formulation," *Computer Methods in Applied Mechanics and Engineering*, Vol. 120, No. 1–2, 1995, pp. 1–32.

[10]Reddy, J. N., "On Refined Computational Models of Composite Laminates," *International Journal for Numerical Methods in Engineering*, Vol. 27, No. 2, 1989, pp. 361–382.

[11]Reddy, J. N., "A Simple Higher-Order Theory for Laminated Composite Plates," *Journal of Applied Mechanics*, Vol. 51, No. 4, 1984, pp. 745–752.

[12]Reddy, J. N., and Liu, C. F., "A Higher-Order Shear Deformation Theory of Laminated Elastic Shells," *International Journal of Engineering Science*, Vol. 23, No. 3, 1985, pp. 319–330.

[13]Reddy, J. N., "A Generalization of Two Dimensional Theories of Laminated Composite Plates," *Communications in Applied Numerical Methods*, Vol. 3, No. 3, 1987, pp. 173–180.

[14]Di Sciuva, M., "An Improved Shear-Deformation Theory for Moderately Thick Multilayered Anisotropic Shells and Plates," *Journal of Applied Mechanics*, Vol. 54, No. 3, 1987, pp. 589–596.

[15]Di Sciuva, M., "Bending, Vibration and Buckling of Simply Supported Thick Multilayered Orthotropic Plates: An Evaluation of a New Displacement Model," *Journal of Sound and Vibration*, Vol. 105, No. 3, 1986, pp. 425–442.

[16]Varadan, T. K., and Bhaskar, K., "Bending of Laminated Orthotropic Cylindrical Shells—An Elasticity Approach," *Composite Structures*, Vol. 17, No. 2, 1991, pp. 141–156.

[17]Ren, J. G., "Exact Solutions for Laminated Cylindrical Shells in Cylindrical Bending," *Composite Science and Technology*, Vol. 29, No. 3, 1987, pp. 169–187.

[18]Xavier, P. B., Lee, K. H., and Chew, C. H., "An Improved Zigzag Model for the Bending of Laminated Composite Shells," *Composite Structures*, Vol. 26, No. 3–4, 1993, pp. 123–138.

[19]Cheng, Z. Q., He, L. H., and Kitipornchai, S., "Influence of Imperfect Interfaces on Bending and Vibration of Laminated Composite Shells," *International Journal of Solids and Structures*, Vol. 37, No. 15, 2000, pp. 2127–2150.

[20]Kim, J. S., and Cho, M., "Efficient Higher-Order Shell Theory for Laminated Composites with Multiple Delaminations," *AIAA Journal*, Vol. 41, No. 5, 2003, pp. 941–950.

[21]Zienkiewicz, O. C., *The Finite Element Method*, McGraw–Hill, New York, 1977.

[22]Cantin, G., and Clough, R. W., "A Curved Cylindrical Shell Finite Element," *AIAA Journal*, Vol. 6, No. 6, 1968, pp. 1057–1062.

[23]Başar, Y., Ding, Y., and Shultz, R., "Refined Shear-Deformation Models for Composite Laminates with Finite Rotations," *International Journal of Solids and Structures*, Vol. 30, No. 19, 1993, pp. 2611–2638.

[24]Balah, M., and Al-Ghamedy, H. N., "Finite Element Formulation of a Third-Order Laminated Finite Rotation Shell Element," *Computers and Structures*, Vol. 80, No. 26, 2002, pp. 1975–1990.

[25]Nayak, A. K., Moy, S. J., and Shenoi, R. A., "Free Vibration Analysis of Composite Sandwich Plates based on Reddy's Higher-Order Theory," *Composite Part B: Engineering*, Vol. 33, No. 7, 2002, pp. 505–519.

[26]Zienkiewicz, O. C., Taylor, R. L., and Too, J. M., "Reduced Integration Techniques in General Analysis of Plates and Shells," *International Journal for Numerical Methods in Engineering*, Vol. 3, No. 2, 1971, pp. 275–290.

[27]Stolarski, H., and Belytschko, T., "Membrane Locking and Reduced Integration for Curve Elements," *Journal of Applied Mechanics*, Vol. 49, No. 1, 1982, pp. 172–176.

[28]Hinton, E., and Huang, H. C., "A Family of Quadrilateral Mindlin Plate Elements with Substitute Shear Strain Fields," *Computers and Structures*, Vol. 23, No. 3, 1986, pp. 409–431.

[29]Dvorkin, E., and Bathe, K. J., "A Continuum Mechanics Based Four-Node Shell Element for General Nonlinear Analysis," *Engineering Computations*, Vol. 1, March 1984, pp. 77–88.

[30]Simo, J. C., and Rifai, M. S., "A Class of Mixed Assumed Strain Methods and the Method of Incompatible Modes," *International Journal for Numerical Methods in Engineering*, Vol. 29, No. 8, 1990, pp. 1595–1638.

[31]Pontaza, J. P., and Reddy, J. N., "Mixed Plate Bending Elements Based on Least-Squares Formulation," *International Journal for Numerical Methods in Engineering*, Vol. 60, No. 5, 2004, pp. 891–922.

[32]Green, A. E., and Zerna, W., *Theoretical Elasticity*, 2nd ed., Clarendon, Oxford, 1968.

[33]Naghdi, P. M., "Foundations of Elastic Shell Theory," *Progress in Solid Mechanics*, Vol. 4, North-Holland, Amsterdam, 1963, pp. 1–90.

[34]Librescu, L., *Elastostatics and Kinetics of Anisotropic and Heterogeneous Shell-Type Structures*, Noordhoff, Leyden, The Netherlands, 1975.

[35]Schmidt, R., and Reddy, J.N., "A Refined Small Strain and Moderate Rotation Theory of Elastic Anisotropic Shells," *Journal of Applied Mechanics*, Vol. 55, No. 3, 1988, pp. 611–617.

[36]Koiter, W. T., "A Consistent First Order Approximation in the General Theory of Thin Elastic Shells," *Proceedings of the Symposium on Theory of Thin Elastic Shells*, North-Holland, Amsterdam, 1960, pp. 12–32.

[37]Büchter, N., and Ramm, E., "3D-Extension of Nonlinear Shell Equations based on the Enhanced Assumed Strain Concept," *Computational Methods in Applied Science*, Elsevier Science, Amsterdam, 1992, pp. 55–62.

[38]Simo, J. C., Rifai, M. S., and Fox, D. D., "On a Stress Resultant Geometrically Exact Shell Model. Part IV: Variable Thickness Shells with Through-the-Thickness Stretching," *Computer Methods in Applied Mechanics and Engineering*, Vol. 81, No. 1, 1990, pp. 91–126.

[39]Reddy, J. N., *Mechanics of Laminated Composite Plates and Shells: Theory and Analysis*, 2nd ed., CRC Press, Boca Raton, FL, 2004.

[40]Reddy, J. N., *Energy Principles and Variational Methods in Applied Mechanics*, Wiley, New York, 2002.

[41]Palazotto, A. N., and Dennis, S. T., *Nonlinear Analysis of Shell Structures*, AIAA Education Series, AIAA, Washington, DC, 1992.

[42]Brebbia, C., and Connor, J., "Geometrically Nonlinear Finite Element Analysis," *Journal of Engineering Mechanics*, Vol. 95, No. 2, 1969, pp. 463–483.

[43]Scordelis, A. C., and Lo, K. S., "Computer Analysis of Cylindrical Shells," *Journal of American Concrete Institute*, Vol. 61, No. 5, 1964, pp. 539–560.

[44]Gibson, J. E., *The Design of Cylindrical Shell Roofs*, Spon, London, 1961.

[45]Ashwell, D. G., "Strain Elements, with Applications to Arches, Rings and Cylindrical Shells," *Finite Elements for Thin Shells and Curved Members*, Wiley, London, 1976, Chap. 6.

[46]Flügge, W., *Stresses in Shells*, 2nd ed., Springer-Verlag, Berlin, 1973.

[47]Kreja, I., Schmidt, R., and Reddy, J. N., "Finite Elements Based on a First-Order Shear Deformation Moderate Rotation Theory with Applications to the Analysis of Composite Structures," *International Journal of Non-Linear Mechanics*, Vol. 32, No. 6, 1997, pp. 1123–1142.

[48]Heppler, G. R., and Hansen, J. S., "A Mindlin Element for Thick and Deep Shells," *Computer Methods in Applied Mechanics and Engineering*, Vol. 54, No. 1, 1986, pp. 21–47.

K. Shivakumar
Associate Editor